Optimizing soybean water use and nitrogen fixation to improve productivity under climate change

A THESIS

SUBMITTED TO THE FACULTY OF THE

UNIVERSITY OF MINNESOTA

BY

Daniel Monnens

IN PARTIAL FULFILLMENT OF THE REQUIREMENTS

FOR THE DEGREE OF

MASTER OF SCIENCE

Under the Supervision of Dr. Walid Sadok

July 2021

Optimizing soybean water use and nitrogen fixation to improve productivity under climate change

Daniel Monnens, M.S.
University of Minnesota, 2021

Abstract

Climate change effects are driving crop yield decreases globally, and yield penalties are often associated with increases in frequency and intensity of heat waves and soil moisture deficits, particularly during reproductive development. Additionally, climate change is driving increases in vapor pressure deficit (VPD) in recent decades, suggesting global atmospheric drying. In a U.S. study, VPD during reproductive stages was identified as the most important predictor of soybean yield variation. Investigations into the effect of VPD on soybean yields often consider its effect on crop transpiration rate (TR) and gas exchange, and such efforts have led to development of drought-tolerant soybean cultivars, which take advantage of particular TR responses to VPD. Despite such progress, no studies have yet examined the effect of VPD on nitrogen fixation, likely due to difficulties of taking non-invasive, real-time measurements.

A common technique for monitoring nitrogen fixation rates non-destructively is the acetylene reduction assay (ARA), which has received critiques due to hazards posed to researchers and potential effects on root nodules. The first goal of this investigation was to develop an alternative method for non-invasively measuring nitrogen fixation that minimizes the above difficulties. A system was designed that enabled us to quantify N_2 fixation as a function of the rate of by-product hydrogen gas (H_2) production by soybean nodules. A second goal was to examine rates of nitrogen fixation in relation to concurrent changes in environmental variables, namely VPD and temperature.

The system was successfully tested on two soybean genotypes in both field and controlled environment conditions. A key result is the confirmation of H_2 production being associated with root nodules, seen by a lack of H_2 signal from plants without nodules. Additional key observations include increases in H_2 production rate from the morning to afternoon in the field, driven at least partly by increases in VPD, consistent with H_2 production rate increases observed when shifting from low to high VPD in a controlled environment. Consistent genotypic differences were observed in both settings, signifying potential for genotypic diversity, which could be exploited in breeding efforts. This study invites further research into the effect of VPD and temperature on N fixation, as soybean growing environments continue to undergo increases in atmospheric drying.

A second focus of this research on soybean is centered on plant water use, which is largely driven by evaporative demand as VPD increases drive increases in TR. Increased TR drives processes beneficial to carbon fixation, so in an environment where available water is not limiting, such behavior should lead to higher yield, or at least be neutral. However, in a water-deficit prone environment, genotypes exhibiting lower TR at high VPD will outperform those exhibiting a 'profligate' TR, by reducing the amount of water lost during the time of day when evaporative demand is the highest. Despite progress in phenotyping soybean TR responses to VPD, so far no QTL have been detected for traits directly reflecting such response curves, due to methodological and logistical challenges. The QTL mapping performed here resulted in the detection, for the first time, of two QTL for the response of TR to both low and high VPD. If confirmed, these QTL could be leveraged to design soybean varieties that are optimized for specific water availability regimes in order to maximize productivity.

TABLE OF CONTENTS

LIST OF TABLES

LIST OF FIGURES

LIST OF ABBREVIATIONS

A	Assimilation Rate
d	Day
DAS	Days After Sowing
E	Transpiration Rate (leaf level)
Exp.	Experiment
g	Grams
g_{sw}	Stomatal Conductance
H_2	Hydrogen Gas
Hrs	Hours
kPa	Kilopascals
LOD	Logarithm of the Odds
m	Meter
mg	Milligrams
Mins	Minutes
mL	Milliliter
N	Nitrogen
N_2	Dinitrogen
NAM	Nested Association Mapping
PAR	Photosynthetically Active Radiation
ppm	Parts Per Million

Prod.	Production
PVC	Polyvinyl Chloride
QTL	Quantitative Trait Loci
RH%	Relative Humidity
RIL	Recombinant Inbred Line
rpm	Rotations Per Minute
s	Second
SNP	Single Nucleotide Polymorphism
T	Temperature
TR	Transpiration Rate (whole-plant level)
umol	Micromoles
VPD	Vapor Pressure Deficit
ΔCO2	Difference in CO_2
ΔH2O	Difference in H_2O

Chapter I:

Nitrogen fixation response to evaporative demand in soybean

1. Introduction

It is now well-documented that climate change is driving crop yield decreases in major agricultural hotspots across the globe (Ray et al., 2019; Mourtzinis et al., 2015; Lobell et al., 2011). In soybean, it has been estimated that 12.4% of potential yields have been lost to climate change-driven environmental stressors between 1961 and 2014 (Matiu et al., 2017). In the literature, a large segment of such yield penalties is associated with historical increases in the frequency and intensity of heat waves and soil moisture deficits stresses, particularly if such effect take place during the critical window of reproductive development (Wijewardana et al., 2018; Zampieri et al., 2017; Zipper et al., 2016; Chenu et al., 2013; Teixeira et al., 2013).

In the case of soybean, the vulnerability of nitrogen (N) fixation towards these environmental stressors constitutes an additional yield-limiting factor, particularly due to the sensitivity of this process to decreasing soil moisture availability. It has been shown, for instance, that nitrogen fixation in soybean declines substantially even under transient soil moisture deficits, where transpiration rate and photosynthesis were not inhibited (Sinclair, 1986; Durand et al., 1987). In a study of drought stress where soybean plants were subjected to progressive soil drying, nitrogen fixation began to decline when only 20% of soil moisture was depleted, as opposed to transpiration rate, which did not decrease until nearly 60% of soil moisture was used (Sall and Sinclair, 1991; Serraj and Sinclair, 1997). This sensitivity appears to be the result of a feedback inhibition mechanism arising from the accumulation of fixed N in the form of ureides in the nodules, which inhibits nitrogen fixation (Figure 1; Sinclair and Serraj, 1995;

Vadez et al., 2000; King and Purcell, 2005). Genotypic variability has been observed for delayed nitrogen fixation decline in response to soil drying, and has been leveraged to produce genotypes with superior yields under moderate to high levels of water deficit (Sinclair et al., 2007).

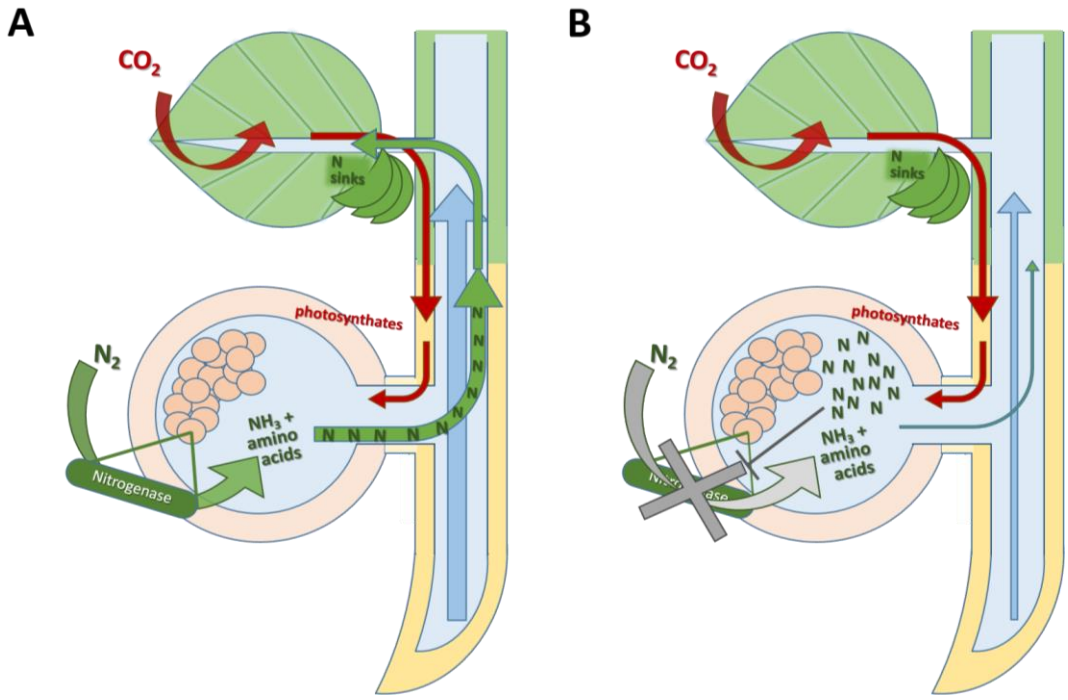

Figure 1. Diagram of symbiotic nitrogen fixation in a soybean nodule (A) where rhizobia within bacteroids fix atmospheric dinitrogen (N_2) via nitrogenase enzymes. Fixed N compounds are then transported to N sinks via the xylem. When fixed N compounds accumulate in the nodule, nitrogen fixation feedback inhibition occurs (B).

In addition to its effects on precipitation and temperature, recent evidence indicates that climate change is driving a phenomenon of atmospheric drying that started in the late 1990s (Ficklin and Novick, 2017, Liu and Sun, 2017; Dai et al., 2018; Yuan et al., 2019). This phenomenon is the result of an increase in atmospheric vapor pressure deficit (VPD), an environmental variable that reflects the difference in

water vapor pressure at saturation (e_s, kPa), and the actual water vapor pressure (e_a, kPa) for a given temperature. The variable e_s is driven essentially by temperature and represents the amount of water the air can hold at saturation, while e_a is dependent on the amount of air moisture, which is the consequence of complex hydrological and global circulation processes. While the exact causes for the global increase in VPD are complex and not very well-understood, they likely involve a rapid increase in e_s as a result of air warming and a relatively slower increase in e_a as a result of limitations to evapotranspiration due to decreased soil moisture or reduced stomatal conductance (Jung et al., 2010; Ficklin and Novick, 2017). The extent of this phenomenon is such that it is expected to offset beneficial effects of CO_2 fertilization (Yuan et al., 2019). Consistently with this, a meta-analysis conducted on soybean yield data in 27 U.S. states during the 2007-2016 period found that VPD during 61 to 90 DAS was the most important predictor of soybean yield across all states (Mourtzinis et al., 2019).

The mechanistic basis of the effect of VPD on soybean yields is often investigated based on well-established quantitative biophysical relationships describing its effect on crop TR and gas exchange (Tanner and Sinclair, 1983; Sinclair 2012; Tardieu et al., 2018). This framework has been successfully used to develop and release superior drought-tolerant soybean cultivars taking advantage of particular TR response curves to VPD (Fletcher et al., 2007; Sadok and Sinclair, 2010b; Carter et al., 2016; Sinclair et al., 2017; Ye et al., 2020; see Chapter 2).

Despite this progress, there are, so far, no studies that examined the effect of daily variation in VPD on the process of nitrogen fixation. A systematic review on the

physiological basis of plant response to VPD by Lopez et al. (2021) conducted on 112 species and 56 traits found no evidence of this relationship being investigated in papers released over the last 50 years. Such lack of progress is likely in part the result of the inherent difficulties to non-invasively measuring dynamic changes in nitrogen fixation.

The most widely used technique for monitoring nitrogen fixation rates non-destructively is the acetylene reduction assay (ARA), a method commonly used to assess the activity of dinitrogenase, which in the absence of dinitrogen will instead reduce acetylene to ethylene (Hardy et al., 1968). This method, widely used in the 70s to 90s, has received critiques and concerns. The primary drawback to ARA, aside from requirement of specialized equipment and chemicals, is the highly flammable nature of acetylene gas that is required (Parsons et al., 1992; Hunt and Layzell, 1993). Additionally, acetylene may affect roots and nodules in an unnatural way that alters physiological function, potentially introducing inaccuracy into measurements of nitrogenase activity (Minchin et al., 1983; Minchin et al., 1986; Silvester et al., 1989). This includes the potential inhibition of nitrogenase by acetylene (Vessey 1994) and the potential for endogenously formed ethylene (Smercina et al., 2019). An additional challenge arises from the difficulty of imposing contrasted VPD regimes independent of confounding environmental variables (Grossiord et al., 2020, Lopez et al., 2021).

To address these limitations, a first goal of this investigation was to develop an alternative method for measuring non-invasively nodule nitrogen fixation that minimizes the above difficulties. To this end, we designed a system that enabled us to

quantify nitrogen fixation as a direct function of the rate of hydrogen (H_2) gas production by the nodules, based on a technique initially developed by Witty (1991). The system was successfully tested on two contrasting soybean genotypes in both field (two soil types) and controlled environment conditions. A second goal was to examine the measured rates of nitrogen fixation in relation to concurrent changes in environmental variables, with a particular emphasis on changes in VPD alone or in interaction with temperature using an ad-hoc VPD control system (Tamang et al., 2019). Additionally, measurements of gas exchange variables (transpiration, stomatal conductance and photosynthesis) and root mass, nodule number and fresh mass were conducted to examine the interplay between canopy gas exchange and nitrogen fixation. We hypothesized that increases in VPD under well-watered conditions would drive an increase in nitrogen fixation rates by down-regulating the dinitrogenase feedback inhibition mechanism.

2. Materials and methods

2.1. Plant material

Two soybean (*Glycine max.*) genotypes were used in the study, consisting of MN1312CN, a public line Released by the University of Minnesota Agricultural Experiment Station in 2014, and CZ1418LL, a high-yielding commercial variety released by Credenz® Soybeans in 2018 (BASF Corporation, Ludwigshafen, Germany). These genotypes were selected based their ability to grow well in PVC

tubes planted in the field (see next section) in a preliminary trial that included an original group of 15 genotypes.

2.2. Field experiment

2.2.1 Planting and growth conditions

Single-row soybean plots (3.7-m rows replicated six times per genotype) were machine-planted at the University of Minnesota field plots on the St. Paul campus on June 5th, 2018. Following planting, 30 cm-long polyvinyl chloride (PVC) tubes of 10-cm diameter were inserted into the center of each plot. These tubes are part of the set-up designed for measuring nitrogen fixation (see next section). Half of these were hammered directly into the soil and therefore contained native field soil, while the other half were placed into dug out holes and filled with coarse sand. Three seeds per genotype were manually planted inside of the PVC tubes at a depth of 2.5cm and plants were thinned 14 days after germination. The day after planting, all tubes were inoculated with rhizobia suspended in nitrogen-free nutrient solution. This consisted of a mixture of two rhizobial strains native to local MN field soils. The inoculation was repeated a second time one week later as seedlings emerged. One such rhizobial strain was used to inoculate seedlings in controlled environment experiments.

To supplement soil nutrients that were unavailable to the seedlings in sand tubes, a nitrogen-free nutrient solution was prepared based on Fujikake et al. (2002) and applied to sand tubes once per week. This nutrient solution was given to the sand tubes for nine weeks after planting until the roots were growing freely out of the

bottom of the PVC tubes and directly accessing field soil. Plants grown in sand-filled tubes were watered every 2 days on average throughout the season to minimize the risk of soil moisture deficit. From date of sowing through the end of the experiment, plants grew under conditions reported in Figure 2 and Table 1.

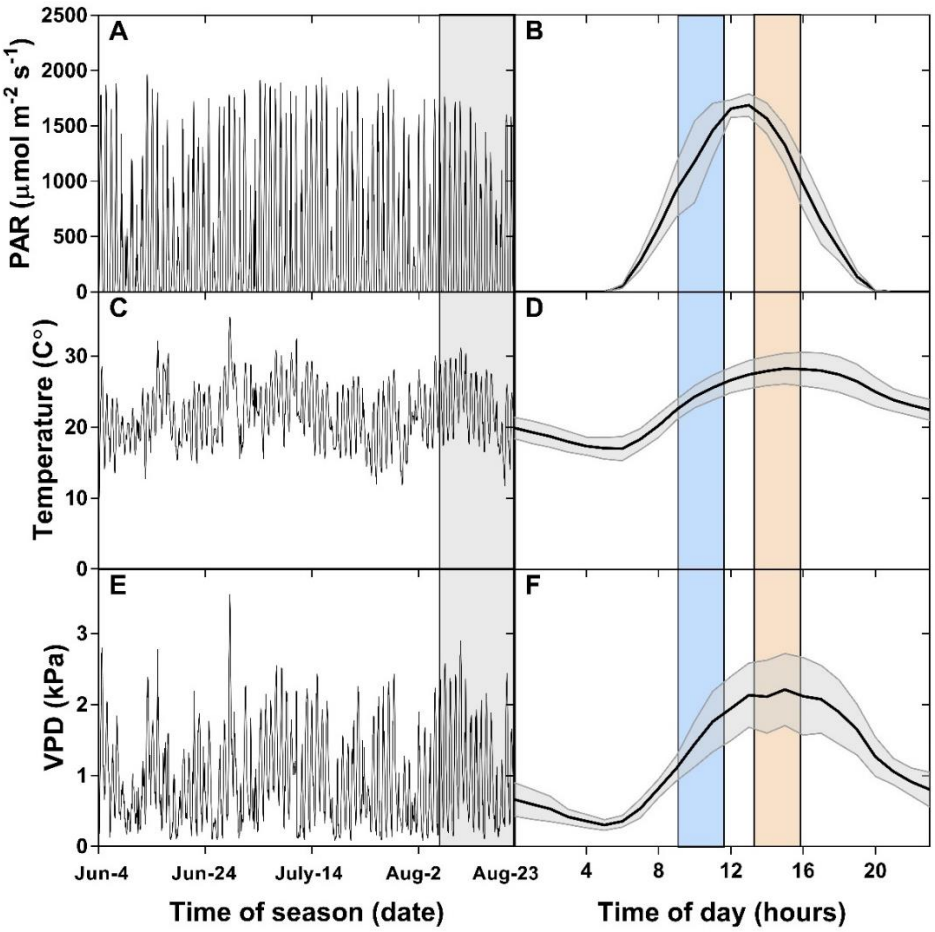

Figure 2. Time courses of photosynthetically active radiation (PAR) (panel A-B), temperature (panel C-D), and vapor pressure deficit (panel E-F) over the growing season (left panels) and during the six H_2 sampling days (right panels) which occurred in the shaded period of the left-hand panels. Shaded areas on the right-hand panels show periods of the day when H_2 sampling occurred during the six sampling days. The black line and grey areas represent the mean and standard errors, respectively. Data was obtained from the Baker Observatory weather station at the St. Paul Campus of the University of Minnesota.

Table 1. Average growth conditions for all four experiments (referred to as Exp1-Exp4). Daytime and nighttime conditions are shown for temperature (T), relative humidity (RH%), and vapor pressure deficit (VPD) with standard errors (SE). Photosynthetically active radiation (PAR) is reported for the daytime only as it is zero during the nighttime.

		Daytime				Night-time		
Exp.	**Environment**	**T (°C) ± SE**	**RH (%) ± SE**	**VPD (kPa) ± SE**	**PAR (µmol m^2 s^{-1}) ± SE**	**T (°C) ± SE**	**RH (%) ± SE**	**VPD (kPa) ± SE**
Exp1	Field	24.0 ± 0.3	59.5 ± 1.4	1.3 ± 0.1	901 ± 34	18.9 ± 0.3	79.4 ± 1.1	0.5 ± 0.0
Exp2	Growth chamber	25.1 ± 0.1	46.9 ± 1.1	1.7 ± 0.0	455 ± 1	18.2 ± 0.1	66.8 ± 1.5	0.7 ± 0.0
Exp3	Growth chamber	25.1 ± 0.1	53.2 ± 0.3	1.5 ± 0.0	455 ± 2	18.2 ± 0.1	74.9 ± 0.1	0.5 ± 0.0
Exp4	Growth chamber	24.9 ± 0.0	55.1 ± 0.4	1.4 ± 0.0	451 ± 1	18.0 ± 0.0	75.4 ± 0.0	0.5 ± 0.0

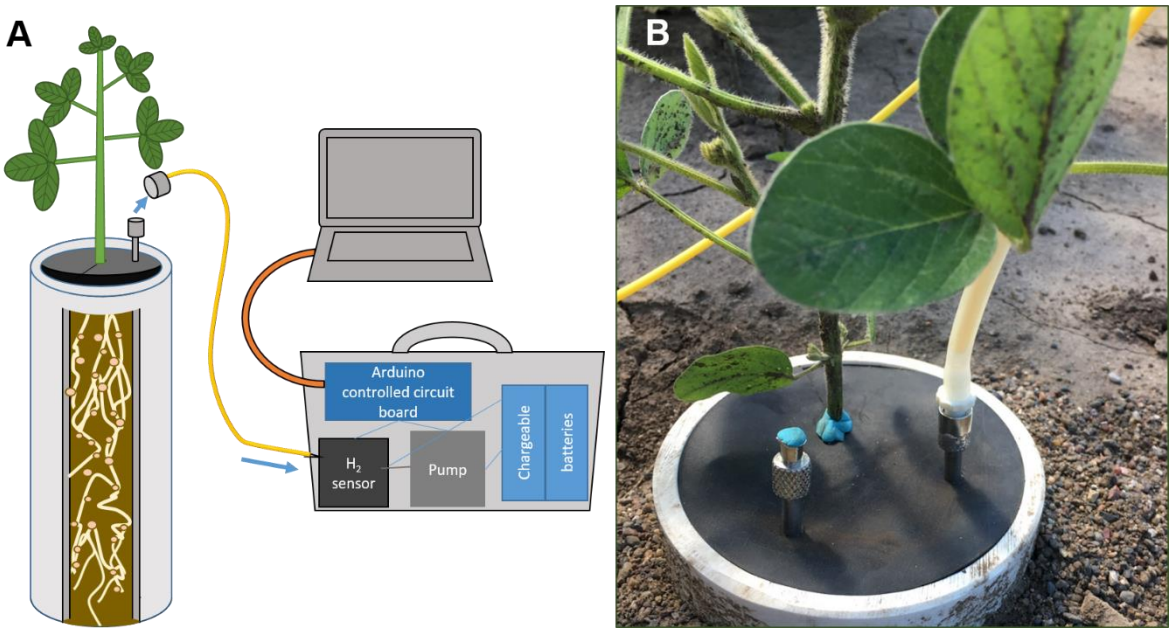

Figure 3. Diagram for the field-based nitrogen fixation measurement system (panel A) with a close-up of the root chamber deployed in the field (panel B). The components of the system are as follows: 1, laptop for recording the data; 2, the H_2 sensing system; and 3, the root chamber planted in the soil (PVC tube, rubber gasket and connector to the pump hose).

2.2.2. In situ measurement of root system H_2 production rate

A portable contraption was built to quantify rates of nitrogen fixation by soybean roots. This device enables direct sensing of hydrogen gas (H_2), a byproduct of the nitrogenase reaction, to determine the rate of nitrogen fixation in real-time, a methodology pioneered by Witty (1991) and further developed by Oono and Denison (2010). The system uses an air pump connected to a H_2 sensor that are controlled by an Arduino circuit board and software that enable the user to control settings for pump speed and sampling interval. The device is versatile, making it possible to quantify H_2 levels on plants grown under field and growth chamber conditions as illustrated in Figure 3.

Under field conditions, the H_2 sensing device was connected to the root system's environment following a technique that was previously successfully used for tracking nitrogen fixation using the acetylene reduction assay under field conditions (Denison et al. 1983). The length of the PVC tube (30 cm) was designed to be twice as long as the original design which ensured that air sampling covered most of the nitrogen fixing rhizosphere. When plants grown in the PVC tube reached the desired growth stage (R1-R3), 2 cm-thick lids made of rubber were sealed around the stem. The middle of this lid presented a 1-cm diameter hole to fit around the stem of the plant, and the lid was partially cut in a straight line from the periphery to central hole to enable installation and removal. The lid dimensions were such that it was tightly sealed around the stem and the PVC tube walls, ensuring that sampled air came from the root environment. Another 2-mm hole was drilled through the lid to enable the

installation of a small metal tube topped with a male Luer lock fitting, to which a female Luer fitting connected to the H_2 sensing equipment via a 1-m long nylon tube (0.125-cm diameter, Figure 3). During measurements, the device was run from a laptop and H_2 production rates could be monitored in real time.

Measurements on the two selected genotypes began approximately 2 months after planting, taking place over three consecutive weeks (stages R1-R3), every 4 days on average, under conditions reported on Table 2. This yielded six sampling days where two genotypes were screened for root H_2 production twice per day, once in the morning (9:00-12:00) and afternoon (13:00-16:00). In each round of measurements, both sand and native soil tubes were measured, for a total of 132 measurements (2 genotypes × 3 replications × 2 soil types), as one afternoon H_2 sampling was not conducted due to a device malfunction.

Table 2. Temperature (T), vapor pressure deficit (VPD), and photosynthetically active radiation (PAR) conditions during H_2 measurement days in the field. Data was obtained from Baker Observatory weather station at the University of Minnesota, St. Paul campus. Morning and afternoon data are averaged (± SE) from 9:00 h to 12:00 h, and 13:00 h to 16:00 h, respectively.

	Morning values			**Afternoon values**		
Date	**T (°C) ± SE**	**VPD (kPa) ± SE**	**PAR (µmol $m^{-2}s^{-1}$) ±SE**	**T (°C) ±SE**	**VPD (kPa) ±SE**	**PAR (µmol $m^{-2}s^{-1}$) ±SE**
Aug-6	21.0 ± 0.6	0.6 ± 0.1	838 ± 265	25.4 ± 0.4	1.6 ± 0.1	1431 ± 187
Aug-8	25.3 ± 1.1	1.4 ± 0.2	524 ± 144	29.6 ± 0.2	2.1 ± 0.1	1462 ± 160
Aug-10	25.9 ± 1.0	1.8 ± 0.3	477 ± 149	29.0 ± 0.2	2.5 ± 0.0	1508 ± 136
Aug-13	27.7 ± 1.0	2.0 ± 0.3	534 ± 145	30.9 ± 0.2	2.8 ± 0.1	1470 ± 125
Aug-15	24.1 ± 0.8	1.2 ± 0.1	527 ± 147	27.3 ± 0.2	1.7 ± 0.0	1368 ± 146
Aug-23	22.2 ± 0.7	1.4 ± 0.1	532 ± 132	24.5 ± 0.1	1.6 ± 0.0	1089 ± 204

During measurements, the pump speed was set identically for each sampling day and the sampling interval was always set to one second, with each measurement lasting for a total of 270 s. Prior to measurement initiation, the pump was run for 90 s, sampling ambient air around the lid of the tube. At the 90-s mark, the female Luer fitting at the end of a silicone tube connected to the H_2 sensing equipment (Figure 3) was rapidly connected to the lid-mounted gasket, which enabled an airtight seal around the plant stem and the inner rim of the tube, and sampling then ran for 180 s.

In nearly all cases, H_2 concentration dynamics followed a sigmoidal time course where ambient air H_2 concentration reading was at a steady-state before sampling began, after which they progressively increased to reach a new plateau (Figure 4). The baseline steady-state measured prior to pump attachment varied depending on the day and was attributed to the amount of water vapor in the air sampled by the system, based on observations in the growth chamber during high humidity conditions where ambient air measurements resulted in higher H_2 sampling baselines. Because of this, this value was subtracted in computing values for actual H_2 production from the rhizosphere each time a measurement took place (see data analysis).

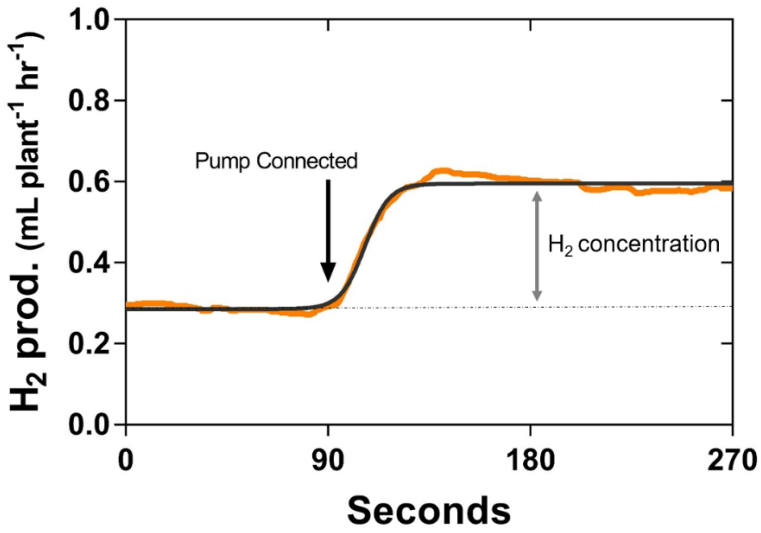

Figure 4. A typical H_2 sampling time course obtained during field measurements (genotype CZ1418LL, grown in sand). The arrow indicates the time when the pump was connected to the root chamber. Raw H_2 data shown in orange with a sigmoidal fitting shown in black. H_2 concentration shown as the difference between sigmoidal plateaus after pump connection.

The increase in the H_2 concentration was attributed to nitrogen fixation by nodules in the soybean root system enclosed in the tube (Denison et al., 1983; Oono and Denison, 2010). Because data from the H_2 sensor is originally expressed in relative units, a transformation of these readings into absolute values (mL H_2 plant^{-1} hour^{-1}) was conducted, based on sensor calibration with a 50-ppm H_2 gas standard (which gives H_2 concentration) and measurements of flow rate (Witty and Minchin, 1998; Walch et al., 2014; Oono et al., 2020). As a result, the rate of H_2 production is given by this equation:

$$H_2 \text{ production rate} = H_2 \text{ concentration} \times \text{flow rate} \qquad \text{(Eq. 1)}$$

Where the flow rates were estimated for both soil types using a flow meter (model FL-1804, Omega Engineering, Norwalk, CT).

2.2.3. Leaf gas exchange measurements in the field

Leaf gas exchange data were concomitantly recorded on two of the six days during which H_2 production assays took place. Measurements were conducted using an LI-6800 Portable Photosynthesis System (LI-COR Inc., Lincoln, Nebraska) with a 3 × 3 cm clear top chamber, a 3 × 3 cm external light source, and a 1 × 3 cm leaf area aperture, such that all leaves covered 100% of the cuvette area. Measurements of stomatal conductance to water vapor (g_{sw}, mol H_2O m^{-2} s^{-1}), transpiration rate (E, mol H_2O m^{-2} s^{-1}) and photosynthetic rate (A, μmol CO_2 m^{-2} s^{-1}) were conducted on the middle section of the middle leaflet of the third trifoliate, twice per day, once in the morning and once after noon. Cuvette conditions were set as follows: [CO_2] = 400 ppm (sample analyzer), flow rate = 500 μmol s^{-1}, fan speed = 10,000 rpm, and overpressure = 0.2 kPa. Temperature and relative humidity were set to track and match the environmental conditions, and the head light source was set to track PAR sensor readings and match the ambient light levels. For each measurement, two stability thresholds had to be met in order to record the considered value. The first stability threshold was sample-to-reference difference in CO_2 levels (ΔCO_2) which slope had to be below 0.7 over a 20 s period. The second stability threshold was the slope of the sample-to-reference difference in water vapor levels (ΔH_2O) which value was set to 0.2 also over a 20 s period.

2.3. Growth chamber experiments

2.3.1. Plant preparation and growth conditions

In addition to the field measurements, three additional experiments (Exp2, Exp3 and Exp4) were conducted on the same two genotypes, this time grown under controlled environment conditions (Table 1). Plants were grown inside a walk-in growth chamber (Model PGV36, Conviron, Controlled Environments Ltd., Winnipeg, Manitoba, Canada) which the following settings: daytime/nighttime temperature = 25/18 °C, daytime/nighttime VPD = 1.5/0.5 kPa, PAR = 450 μmol m^{-2} s^{-1}, photoperiod = 14 hrs (Table 1).

Plants were grown in 50 × 15 cm plastic growth pouches (Cyg seed germination pouch, Mega International of Minneapolis, USA) in which a germination paper was placed to retain moisture, hold seeds, and support plants after germination. The bottom crease of this folded section is serrated with holes that allow roots to easily penetrate and grow into the large rooting area in the growth pouch below.

Prior to placement in the growth pouches, seeds were sprayed with a 70% ethanol solution, soaked in hydrogen peroxide for two minutes, then rinsed in distilled water to ensure sterilization. Two seeds were then placed hilum-down in each pouch to ensure successful germination such that each pouch was thinned to a single healthy plant 10 days after germination. Initially, each pouch received 50 mL of a nutrient solution prepared following Fujikake et al. (2002). A volume of 1 ml of one rhizobial inoculant used in the field experiment (about 2×10^6 rhizobia cells) was added to each pouch at seeding and second time when taproots were approx. 3 cm long. Ten days after seeding, nodulated plants received a nitrogen-free nutrient solution (Fujikake et

al., 2002), two to three times per week. The amount of solution added was calculated based on average daily water loss, which averaged approx. 50 mL per week.

An exception was a group of 8 plants in Exp4, which were not inoculated to confirm that plants without nodules plants do not emit hydrogen (see Results). This run (Exp4) included eight inoculated plants (4 per genotype) watered with the nitrogen-free nutrient solution, and eight non-inoculated plants supplied with the same nutrient solution with supplemental nitrogen provided by the addition of 10 mM ammonium nitrate. In some instances, these plants still presented a very small numbers of nodules, which were removed manually.

Pouches were arranged in a grid container with dividers (DG93120BL Dividable Grid Storage Container, Quantum Storage Systems, Miami, USA), which was rotated twice per week in the chamber, while pouches were rotated once per week within the bin. Three portable sensors were deployed in three locations across the growth chamber to record temperature, relative humidity, and vapor pressure deficit at the plant canopy height every five minutes (EL-USB-2-LCD, Lascar Electronics, Whiteparish, UK). Photosynthetically active radiation (PAR) was recorded via a quantum sensor (HOBO H21-USB micro station, Onset Computer Corporation, Bourne, MA) similarly placed at canopy height in the center of the growth chamber.

2.3.2. Nitrogen fixation response to VPD

The effect of VPD on nitrogen fixation was investigated at two temperatures (25°C, Exp2 & Exp4; and 30 °C, Exp3). At each temperature, the low and high VPD

treatments were imposed based on protocols from Tamang and Sadok (2018) and Tamang et al. (2019). Briefly, at each temperature, the low VPD treatment was achieved using four industrial humidifiers (Model 200H, Hydrofogger LLC., Greenville, South Carolina, USA) which made it possible to maintain a relative humidity (RH) above 80%. The high VPD treatment was imposed after turning off the foggers and activating two industrial dehumidifiers (DRI-EAZ LGR 7000Xli, Legend Brands, Burlington, WA, USA), which were programmed to maintain a RH of 30%.

In each experiment, the sequence started by the low VPD treatment which was initiated in the beginning of the light period (6:00 am), to which plants were exposed for 60 min. Afterwards, nitrogen fixation measurements were conducted under these same conditions for an additional 90 to 120 min. After these measurements were completed, the same plants were then acclimated to the high VPD treatment for the same duration (60 min) after which the high VPD nitrogen fixation measurements were conducted for during the subsequent 90-120 mins following the same sampling order as in the low VPD treatment. Experimental conditions of the controlled environment measurements are compiled in Table 3.

Table 3. Experiment descriptors and environmental conditions during the controlled environment experiments. Two to three runs were performed weekly in a given experiment, requiring two days to complete. Plant age is shown as number of days (d) since planting. Average values for temperature (T), vapor pressure deficit (VPD), and photosynthetically active radiation (PAR) are shown along with their standard error (SE).

					Low VPD			**High VPD**		
Exp.	Run	Planting date	Plant age (d)	Reps	T (°C) ± SE	VPD (kPa) ± SE	PAR (µmol $m^{-2}s^{-1}$) ± SE	T (°C) ± SE	VPD (kPa) ± SE	PAR (µmol $m^{-2}s^{-1}$) ± SE
2	2.1	Apr-23	40	6	25.0 ± 0.1	0.6 ± 0.03	458 ± 5	24.5 ± 0.2	1.9 ± 0.04	455 ± 3
		Apr-23	42	6	24.9 ± 0.1	0.4 ± 0.02	478 ± 3	25.1 ± 0.2	2.1 ± 0.05	444 ± 4
	2.2	Apr-23	47	6	25.0 ± 0.1	0.4 ± 0.02	463 ± 4	24.8 ± 0.2	2.0 ± 0.05	440 ± 3
		Apr-23	48	6	24.9 ± 0.1	0.5 ± 0.03	469 ± 3	25.0 ± 0.1	2.0 ± 0.04	426 ± 3
3	3.1	May-14	33	8	29.4 ± 0.3	0.5 ± 0.03	504 ± 3	29.7 ± 0.1	2.9 ± 0.03	495 ± 3
		May-14	34	8	29.8 ± 0.1	0.8 ± 0.03	488 ± 4	29.7 ± 0.1	3.0 ± 0.04	501 ± 2
	3.2	May-14	40	8	29.8 ± 0.2	0.8 ± 0.04	496 ± 3	30.2 ± 0.1	3.1 ± 0.03	496 ± 2
		May-14	41	8	30.1 ± 0.1	0.9 ± 0.04	495 ± 3	29.6 ± 0.1	3.0 ± 0.04	488 ± 3
	3.3	May-14	47	8	30.2 ± 0.1	0.8 ± 0.05	483 ± 4	30.1 ± 0.1	3.1 ± 0.04	494 ± 1
		May-14	48	8	30.0 ± 0.2	0.9 ± 0.07	482 ± 3	30.2 ± 0.1	3.1 ± 0.03	481 ± 2
4	4.1	July-19	44	4	24.8 ± 0.1	0.3 ± 0.03	461 ± 4	24.7 ± 0.1	1.9 ± 0.04	445 ± 3
		July-19	45	4	25.0 ± 0.0	0.3 ± 0.01	460 ± 6	24.7 ± 0.1	1.9 ± 0.03	440 ± 3
	4.2	July-19	51	4	25.1 ± 0.1	0.7 ± 0.03	443 ± 4	24.9 ± 0.1	2.0 ± 0.03	442 ± 3
		July-19	52	4	25.0 ± 0.1	0.5 ± 0.02	446 ± 4	24.8 ± 0.1	2.0 ± 0.04	447 ± 2
	4.3	July-19	58	4	24.7 ± 0.2	0.6 ± 0.03	428 ± 4	24.9 ± 0.1	2.0 ± 0.03	429 ± 2
		July-19	59	4	25.0 ± 0.1	0.5 ± 0.02	426 ± 5	24.9 ± 0.1	2.0 ± 0.03	433 ± 2

Similar to the field experiment, measurements of nitrogen fixation rates were conducted by tracking rates of H_2 production by the root nodules. This was done using a similar portable H_2 sensing device as the one used in the field experiment, and following the same general approach described earlier, with some modification due to the nature of the controlled environment plant growth setup. Briefly, prior to measurements, the pouches were drained of nutrient solution so that the only moisture remaining is the amount of water adsorbed on root and pouch wall (Noel et al., 1982). This approach was needed to ensure consistent and adequate aeration during each pouch measurement and ensure no nodules are submerged underwater (Serraj and Sinclair, 1996). The H_2 sampling device is connected to the pouch via male-to-female Luer lock fittings attached to a metal tube feeding through a rubber gasket which fits

tightly into the top of the growth pouches (Figure 5). This gasket is inserted into the pouch opening and secured with large binder clips. One metal tube of the gasket is a valve for pump attachment which reaches down to the middle of the pouch, and another is a valve that is an air inlet towards the top of the pouch (Figure 5).

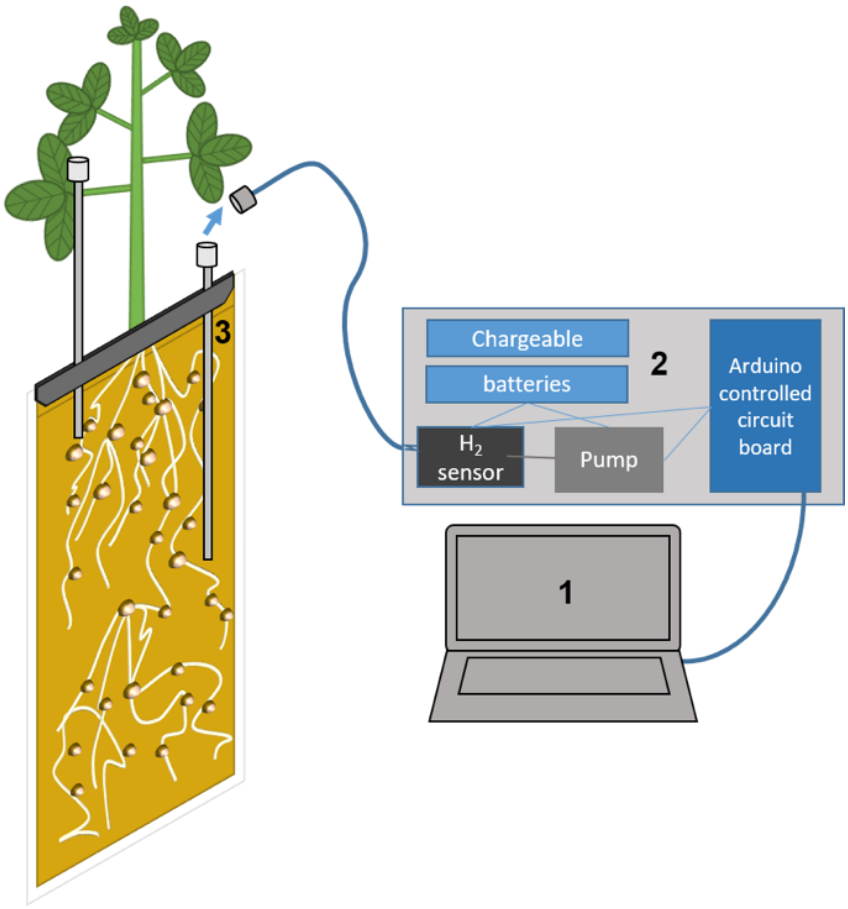

Figure 5. Diagram for the nitrogen fixation measurement system configured for the plant growth pouch set up used in the controlled environment experiment. The components of the system are as follows: 1, laptop for recording the data every second; 2, the H_2 sensing system (Arduino circuit board, H_2 sensor and pump); and 3, the growth pouch set-up (pouch, rubber gasket and two valves). The arrow shows the connection point between the pouch and sampling device, as well as the direction of airflow.

Similar to the field measurements, the pump speed was set identically for each sampling day and H_2 levels were recorded every second. Ambient air was sampled for 60 seconds prior to connecting to instrument to the pouch gasket via Teflon capillary tubing, in order to quantify a baseline H_2 detection. Measurements were then taken for 500s before the process is repeated with the next plant. The longer time for sampling in the controlled environment compared to the field was based on pilot tests for how long it would take for H_2 to reach a steady-state in the growth pouch. After the pump hose was detached, the gasket was removed and sterilized with isopropyl alcohol to prevent the spread of contaminants, and nutrient solution is resupplied. Relative H_2 units were transformed to absolute values (mL H_2 $plant^{-1}$ $hour^{-1}$) as described earlier with a new measurement of flow rate and calibration with a 50 ppm H_2 standard.

2.3.3. Leaf gas exchange response to VPD

Sampling pouch plants for leaf gas exchange variables (A, g_{sw}, E) took place during Exp4 (Exp4.1, Exp4.2, and Exp4.3, Table 3) using the LI-6800 photosynthesis system described earlier after H_2 sampling over the first two days. Measurements under target VPD conditions were conducted in exactly the same way as described in the previous section, i.e., took place after acclimating plants to the low (0.5 kPa) and high (2 kPa) VPD conditions for 60 mins. Like field measurements, gas exchange measurements were conducted on the middle leaflet of the third trifoliate. As in the field experiment, T and PAR cuvette conditions were set to the ambient conditions (T = 25˚C, PAR = 450 μmol m^{-2} s^{-1},) with RH set at 84% and 37% for the low and high

VPD steps, respectively. The same settings were applied ([CO_2] = 400 ppm, flow rate = 500 μmol s^{-1}, fan speed = 10,000 rpm) except that overpressure was set at 0.1 kPa. The same stability thresholds for ΔH_2O and ΔCO_2 were used as pre-conditions for recording values.

2.3.4. Plant size and nodule measurements

Plant phenological stages, total leaf areas, shoot and root dry mass, and nodule traits were determined for all plants in experiments Exp2, Exp2, and Exp4. Nodule numbers and dimensions were estimated using RootPainter image processing software (Smith et al., 2020). Nodule fresh mass was estimated based on root system images taken using an iPhone 6s camera (Apple Inc, Cupertino, California, USA). Based on an assumption of equivalent nodule density and spherical shape, fresh weights were estimated from the nodule volume which was determined based on nodule diameter as calculated by the RootPainter program, a GUI-based software program to rapidly train deep neural networks for use in biological image analysis (Smith et al., 2020), specifically including nodule measurements from root images. Dry mass values were recorded after oven-drying for three days at 60˚C.

2.4. Data analysis

In the case of field-based H_2 time courses, the first 45 s of the 90 s ambient air sampling was removed to avoid potential effects on the baseline calculation, as H_2 readings were occasionally still decreasing from the previous plant sample in the first

30-45 s of the following measurement. Time courses of H_2 production were then fitted with a sigmoidal curve which enabled computing a baseline value for ambient air H_2 (measured prior to connecting the device to the root chamber), and a higher plateau, reflecting steady-state H_2 production by the nodules (example on Figure 4). For each measurement, the actual rate of H_2 production was estimated as value of the high plateau minus the baseline value. This ensured that variation in the 'background noise', which likely occurred as a function of sensible changes in ambient RH within days and between days as H_2 sensors can be sensitive to water vapor, are taken into account to accurately compute H_2 values that reflect nitrogen fixation by the nodules.

In the case of growth chamber data, a one-phase exponential decay model was found to be a better fit for the H_2 time courses after sampling starts. This was primarily due to the presence of a H_2 peak that manifests right as the pump is connected to the pouch gasket due to H_2 buildup in the small pouch volume. The H_2 levels then progressively decrease to a steady-state value, representative of the H_2 production rate by the nodules. Similar to field conditions, steady-state baseline H_2 levels appeared to fluctuate between days and treatments due to differences in RH, and to correct for this effect, an average H_2 baseline value was calculated prior to each measurement, based on the 30 seconds of ambient air sampling immediately prior to pump-pouch attachment. This baseline value was then subtracted from each steady-state H_2 level derived from the one-phase exponential decay model.

Differences between genotypes and treatments were analyzed using parametric t-tests and two-way ANOVAs . Parametric t-tests, regression analyses, and Pearson

correlations were conducted using the statistical software PRISM 7.0c (GraphPad Software Inc., San Diego, CA, 2017), and analyses of variance were carried out using R-based scripts (R Core Team, 2021).

3. Results

3.1. Effect of nodule presence on H_2 production

Due to the impossibility of removing nodules or ensuring that no nodulation took place in field-grown plants, the controlled environment growth pouch set-up was used to confirm that H_2-sensing system captured hydrogen emitted by the roots, and primarily the nodules. As indicated in Figure 6, irrespective of the genotype, concurrent examination of plants with and without nodules exhibited highly significant differences in H_2 production ($P < 0.0001$). Furthermore, H_2 production for plants without nodules was not significantly different from zero for both genotypes, indicating that nodules are primary sources of H_2 production by the root system.

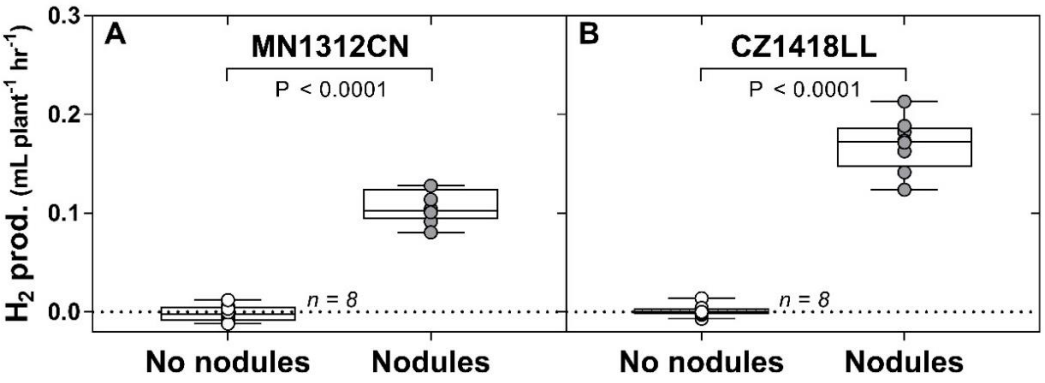

Figure 6. Hydrogen gas (H_2) production from nodulated and non-nodulated plants from genotypes MN1312CN (panel A) and CZ1418LL (panel B). *P*-values shown are the result of unpaired t-tests between plants with no nodules and with nodules where *n* represents the total number of observations.

3.2. Nitrogen fixation and gas exchange response to the environment in the field

Across all measurement days, both genotypes grown in sandy soil consistently exhibited a time-of-day dependent pattern of nitrogen fixation measured as the rate of H_2 production from the roots (Figure 7). As temperature, PAR and VPD increased (Figure 2), H_2 production of plants grown in sand significantly increased during the afternoon, by 60% and 44% for genotypes MN1312CN and CZ1418LL, respectively (Figure 7AB).

A similar pattern was observed for plants grown in native soil, whereby MN1312CN and CZ1418LL exhibited an increase in H_2 production by 22% and 24% during the same time window, but these were not found to be statistically significant (Figure 7CD) due to a larger scatter of the data. Despite H_2 production being significantly lower in plants grown in native soil (66% lower compared to sandy soil, $P < 0.0001$), the trends remained statistically significant when combining data from both soil types (Figure 7EF). In these responses, the genotypic effect was only significant for plants grown in the native field soil, whereby CZ1418LL tended to exhibit a significantly higher rate of H_2 production compared to MN1312CN (46% higher, $P = 0.004$). Overall, and independent from soil type and genotype, H_2 production increased significantly ($P < 0.0001$) by 46% in the afternoon.

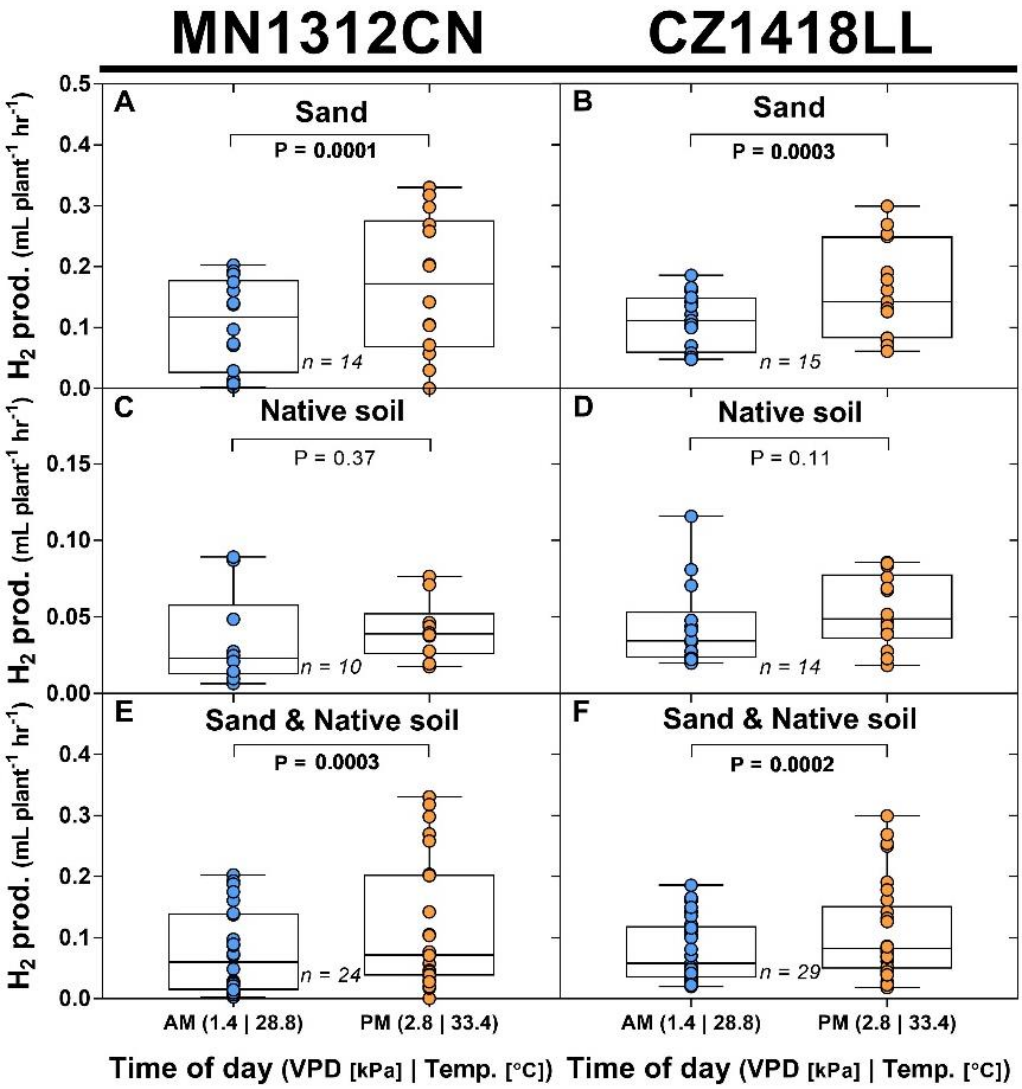

Figure 7. Variation in rates of nitrogen fixation estimated as rates of hydrogen gas production by the roots, as a function of time of day and the corresponding environmental conditions, genotype (MN1312CN, panels A, C and E; CZ1418LL panels B, D and F) and soil type (native soil and sand). In the box-and-whiskers, the box represents the median and the 25th –75th percentiles, while the whiskers represent the largest and smallest values. *P*-values are outputs of paired t-tests between morning (AM) and afternoon (PM) measurements for which VPD (kPa) and temperature (°C) conditions are indicated. *n* represents the total number of observations.

Leaf gas exchange response to changes in environmental conditions as a function of the time of day was found to be relatively consistent across genotypes, particularly for plants grown in sandy soil (Figure 8). In this case, stomatal conductance and photosynthetic rates were unaffected by time of day (not shown), while transpiration rate consistently increased by 65% and 35% in the afternoon relative to the morning for genotypes MN1312CN and CZ1418LL, respectively.

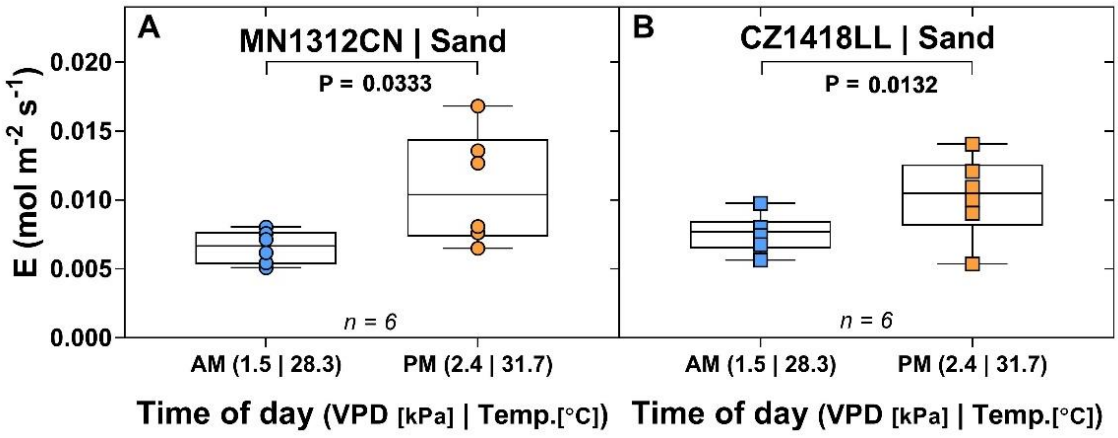

Figure 8. Time-of-day variation in transpiration rates measured in the field using a portable gas exchange system as a function of the genotype (MN1312CN, CZ1418LL). The remaining components of the figure are as described in the caption for Figure 7.

Measurements made on plants grown in native soil were more scattered, resulting in non-significant differences in gas exchange parameters as a function of the time of the day, with the only exception being a decrease in photosynthetic rate for genotype CZ1418LL during the afternoon ($P < 0.05$, not shown). Overall, combining genotypes and soil types, trends converged only for transpiration rate, showing an overall significant increase of 34% during the afternoon ($P = 0.01$).

Due to the scatter of the data and the relatively limited number of observations, there was no significant correlation between gas exchange and H_2 production rates - although in all cases they positively co-trended. The strongest relationship found was a correlation between transpiration rate and H_2 production for plants grown in native soil (P = 0.06, R^2 = 0.25, Figure 9).

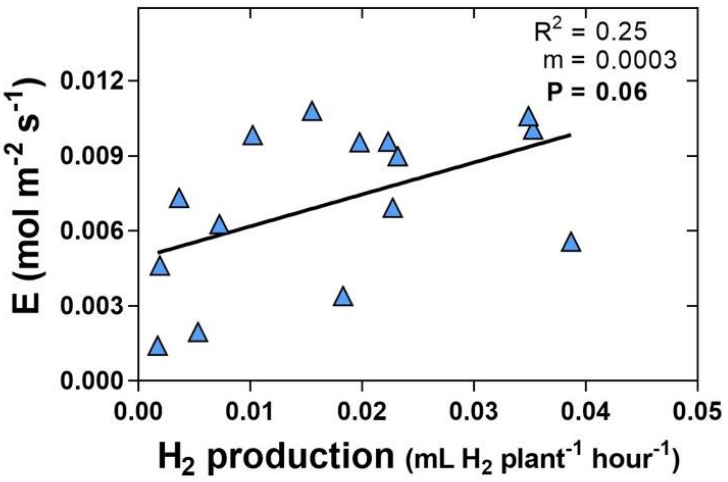

Figure 9. Relationship between nitrogen fixation, quantified as hydrogen gas (H_2) production and transpiration rate (E) measured in the field in native soil. The slope (m), *P*-value and coefficient of determination of the linear regression are indicated.

3.3. Nitrogen fixation and gas exchange response to VPD

Because time-of-day effects on nitrogen fixation was driven by co-occurring changes in temperature and VPD in the field (i.e., Figure 7), the growth chamber experiment was designed to examine these effects separately. As highlighted in Figure 10, the effect of VPD on nitrogen fixation was dependent on temperature, with no interaction with genotypes. A 4-fold increase in VPD from 0.5 to 2 kPa at 25°C did

not result in a change in H_2 production, while a comparable increase (3.75-fold) in VPD from 0.8 to 3 kPa at 30°C translated into a significant increase in root H_2 production by 16% and 25% for MN1312CN and CZ1418LL, respectively (Figure 10). These same tendencies remained identical whether H_2 measurements were normalized based on root mass, nodule number, or nodule fresh mass (not shown).

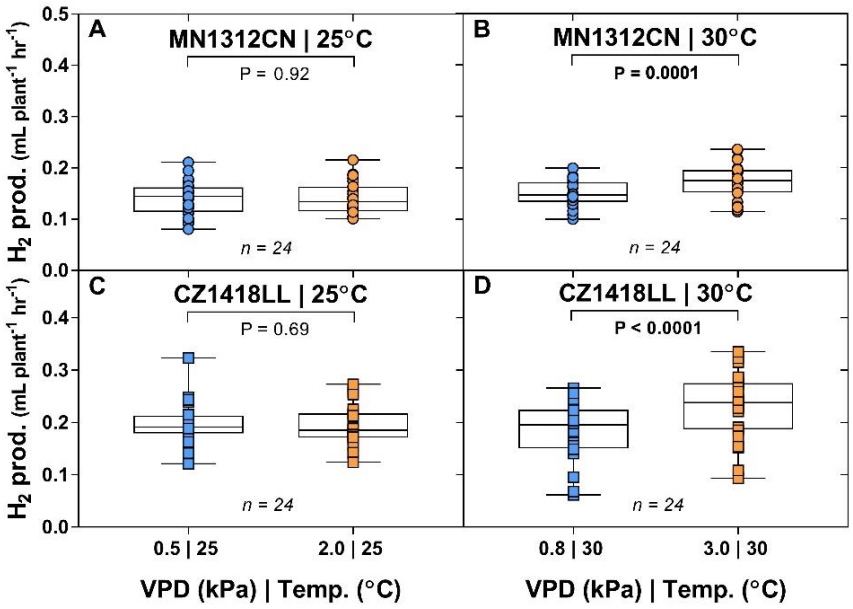

Figure 10. Effect of vapor pressure deficit (VPD) and temperature on nitrogen fixation estimated by measuring hydrogen gas (H_2) production by the nodules under controlled environment conditions. Results are shown separately for the two genotypes, MN1312CN (panels A and B) and CZ1418LL (panels C and D) and two temperature conditions (25˚C, panels A and C; 30˚C, panels B and D). The remaining components of the figure are as described in the caption for Figure 7.

Leaf gas exchange measurements conducted at the low VPD treatment were found to be unreliable due to the condensation on the instrument resulting from fogger treatments. Therefore, only data measured under the high VPD treatment (2 kPa,

25°C) was used in the analysis and data from both genotypes was analyzed jointly given the limited number of observations (Figure 11). Under these conditions, all gas exchange variables positively and significantly correlated with H_2 production rates, with the strongest relationships observed when normalizing H_2 production based on nodule fresh weight (Figure 11).

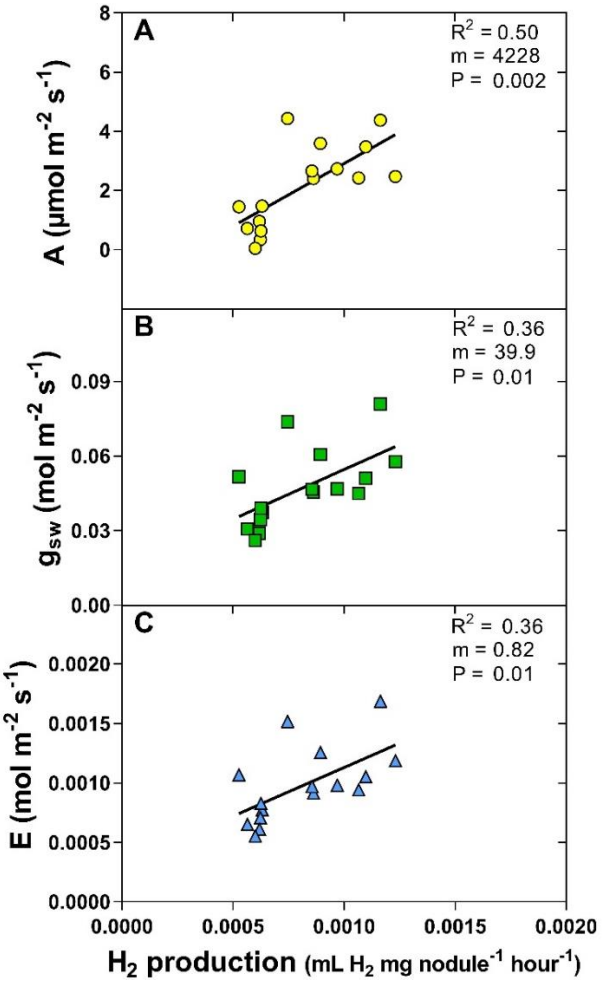

Figure 11. Relationship between nodule H_2 production rate calculated on a nodule fresh mass basis and assimilation rate (A), stomatal conductance (g_{sw}), and transpiration rate (E). The slope (m), coefficient of determination (R^2), and the *P*-value of the regressions are indicated.

3.4. Differences in nitrogen fixation among genotypes

When expressed on a root mass basis (Figure 12A), H_2 production rates were not found to significantly differ between genotypes CZ1418LL and MN1312CN, while normalizing by nodule number (Figure 12B) and fresh mass (Figure 12C) revealed consistent differences in root nitrogen fixation between genotypes. In these cases, and regardless of the VPD and temperature treatments, genotype CZ1418LL consistently exhibited significantly higher rates of nitrogen fixation compared to MN1312CN per nodule (70% higher) and on a nodule fresh mass basis (34% higher).

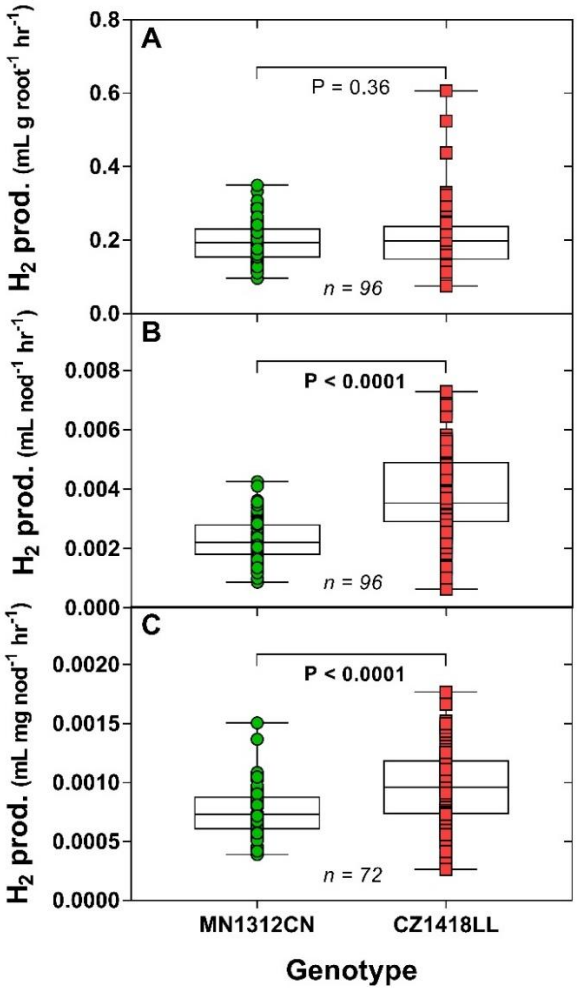

Figure 12. Differences in nitrogen fixation estimated by measuring hydrogen gas (H_2) production by the nodules under controlled environment conditions between the two soybean genotypes MN1312CN and CZ1418LL. H_2 production rates shown as normalized by root dry mass, nodule number, and nodule fresh mass (panels A, B, and C, respectively). In the box-and-whiskers, the box represents the median and the 25^{th} – 75^{th} percentiles, while the whiskers represent the largest and smallest values. *P*-values are outputs of un-paired t-tests between genotypes. Significant results with P-values ≤ 0.05 are bolded. Number of pairs is shown with *n.*

4. Discussion

4.1. Development of a minimally invasive *in situ* method for non-destructively measuring nitrogen fixation in soybean

Direct and 'real time' quantification of the rate of nitrogen fixation by root nodules in the field is a particularly tedious task and as a result, has been a major challenge facing nitrogen fixation research. The hydrogen production assay developed in this investigation, first pioneered by Witty (1991), resolves major limitations typically associated with the more widely used acetylene reduction assay (ARA, Smercina et al., 2019; Vessey, 1994; Minchin et al., 1985, 1983). By simply measuring rates of hydrogen gas production by the nodules, a well-known byproduct of nitrogen fixation (Witty, 1991; Oono and Denison, 2010), the method developed here avoids two major drawbacks often associated with ARA. First, this method does not necessitate the complex logistics of using acetylene, a highly flammable gas, which has been a source of concern (Carson, 2002; Hunt and Layzell, 1993). Second and more importantly, this technique is less invasive, as it resolves the issues of potential inhibition of nitrogenase by acetylene (Vessey 1994) and the endogenous

formation of ethylene gas, which can result in inaccurate estimation of nitrogen fixation as estimated using ARA (Smercina et al., 2019).

While there are limits to the technique used in this study (see next paragraph), several lines of arguments support the premise that the approach proposed was reasonably successful in estimating rates of nitrogen fixation by soybean nodules. Consistent with theory, removing nodules resulted in a nullification of hydrogen production (Figure 6), indicating that they are the primary source of the H_2 gas sampled by the system. Additionally, genotypic differences were consistently observed in these responses (Figures 6 & 12), indicating that the H_2-sensing system is capturing a biological, plant-dependent process, rather than a soil-based process *per se*. Furthermore, trends of root system H_2 production over time in the field were consistent over days, increasing in the afternoon independent of the soil medium, a finding that is consistent with early reports indicating that nitrogen fixation tends to increase in the afternoon (Johnson and Hume, 1972; Denison and Sinclair, 1985).

The main limitation of this approach arises from the potential presence of hydrogen oxidizing bacteria in soils, which could result in weakening the 'signal' of H_2 production by the nodules (Miamaiti et al., 2007; Schuler and Conrad, 1991; La Favre and Focht, 1983). Additionally, the native field soil could have had pre-existing rhizobial populations which could have formed a symbiosis with the planted soybeans, possibly including strains expressing uptake hydrogenase (HUP^+) which recycle H_2 within the nodule (Annan et al., 2012; Godfroy and Dravon, 1991; Evans et al., 1987). Such H_2 signal weakening is supported by our field data, which shows that hydrogen

gas production was lower in plants grown in native soil, compared to those grown in columns filled with sand (Figure 7), and in fact, the use of the sand as an alternative substrate in our experimental design was in anticipation of this possibility. The hypothesized presence of such bacteria in the native soil, did not, however, generate an inconsistent trend in H_2 gas production relative to plants grown in the sand (compare panels A-B and C-D in Figure 7). As a result, pooling nitrogen fixation data from both soil media still confirmed the earlier observations that nitrogen fixation increased in the afternoon (Johnson and Hume, 1972; Denison and Sinclair, 1985).

4.2. Soybean nitrogen fixation responds to evaporative demand

The major finding of my work is the observation that nitrogen fixation in soybean, and presumably other nitrogen-fixing plant species, is responsive to variation atmospheric vapor pressure deficit, at least at a temperature of 30°C (Figure 10BD). If confirmed on other genotypes and species, this result points a much more important, and previously undocumented role of VPD not only on legume yields but also on plant primary productivity and global nitrogen cycling.

A parsimonious explanation for the favorable VPD effect found in this study would be its involvement in regulating nitrogen fixation feedback inhibition arising from the accumulation of ureides and amino acids in nodules, which have been extensively documented in soybean (Serraj et al., 1999; Vadez and Sinclair, 2001; King and Purcell, 2005). This hypothesis is supported by the positive correlation observed between nitrogen fixation and transpiration rate (E) under both field (Figure

9) and controlled environment (Figure 11) conditions. In further support of this hypothesis, the strongest relationship between E and nitrogen fixation found in the pouch experiments was observed when H_2 production was expressed on a nodule fresh mass basis (Figure 11), while expressing on a root mass basis yielded a non-significant correlation.

Feedback inhibition has also been attributed to ureide accumulation in leaves and transport of ureides to the nodule via phloem (Vadez et al., 2000; Bacanamwo and Harper, 1997; Parsons et al., 1993). Increased transpiration rate results in a reduction of organic solute transfer from xylem to phloem (White, 2012), and in soybean this was previously attributed to a decrease in lateral escape of amino acids to xylem parenchyma cells (Da Silva and Shelp, 1990). If the highest VPD treatment (3.0 kPa) where transpiration was presumably the highest (Sinclair and Bennet, 1998) was the only to result in a significant increase in nitrogen fixation rate, a reduction in the transfer of ureides from the xylem to the phloem could have alleviated feedback inhibition and promoted higher levels of nitrogenase activity. This potential link between nitrogen fixation feedback inhibition and transpiration rate is further supported by observations of decreased transpiration resulting in increased accumulation of petiole ureides in well-watered soybean plants (de Silva et al., 1996).

The interplay between VPD and temperature is difficult to dissect in this dataset, as a VPD effect on nitrogen fixation was observed for measurements at 30°C, but not at 25°C. It was proposed by Denison et al. (1988) that the most-direct limitation to nodule respiration, and therefore production of energy needed for

nitrogen fixation, is the flux of oxygen diffusing into nodules. It was subsequently observed that soybean root nodules undergo significant increases in nitrogen fixation, O_2 flux, and O_2 permeability as a result of increased temperature (Kuzma and Layzell, 1994; Weisz and Sinclair, 1988). Therefore, if O_2 flux into the nodule is the limiting factor in supplying the necessary energy for nitrogen fixation as suggested by Denison et al. (1988), then the increase in nitrogen fixation at elevated VPD observed for plants measured at 30°C could be a result of increased diffusion of oxygen into nodules, compared to nodules measured at 25°C.

Alternatively, it is possible that the H_2 increase was observed at 30°C because the high VPD treatment was considerably higher than that at 25°C (3.0 and 2.0 kPa, respectively). When dividing the data into four treatment groups defined by both VPD and temperature conditions (kPa|°C), only the high VPD and high temperature treatment (3.0|30) showed a significant difference in H_2 production. This might be an indication of a VPD threshold, meaning that alleviation of feedback inhibition might take place when VPD is between 2 and 3 kPa. Certainly, gathering more nitrogen fixation data in response to a range of VPD regimes would be useful to address this question.

5. Conclusions and perspectives

Overall, this research presents a successful implementation of a non-invasive, real-time measurement of nitrogen fixation of soybean nodules by direct sensing of hydrogen gas, which avoids logistical and physiological limitations of current

commonly used methods, namely, ARA. As a demonstration of reliability, perhaps the most important result included here is the method validation of our instrument detecting H_2 production specifically from nodules in the root system, as seen by a lack of H_2 signal from plants without nodules.

Through implementation of direct hydrogen sensing in a field and controlled environment setting on two soybean varieties, key observations were made, including differences in H_2 production rate between the morning and afternoon, apparently driven at least partly by increases in VPD. This increase in nitrogen fixation from low to high atmospheric VPD was consistent with observations on plants sampled at 30°C in a controlled environment. Consistent genotypic differences were also observed in both the field and controlled environment, signifying the potential for genotypic diversity of N_2 fixation in soybean which could be exploited in breeding efforts. Additionally, this study invites further research into the effect of VPD and temperature on nitrogen fixation, especially as soybean production environments continue to experience a global increase in atmospheric drying.

Chapter II:

High-throughput phenotyping and QTL mapping of transpiration responses to increasing evaporative demand in a soybean mapping population

Introduction

Climate change is negatively impacting soybean productivity, largely via decreases in water availability during critical reproductive periods, which is the most important environmental factor contributing to loss of crop yield, particularly for soybean (Boyer, 1982; Dai, 2013; Zipper et al., 2016). A key, yet poorly understood driver of climate change-driven water deficits is the increase in atmospheric water vapor pressure deficit (VPD), an environmental variable that drives evaporation from soil and plant canopies (Zhang et al., 2015; Ficklin and Novick, 2017; Yuan et al., 2019). This increase in VPD stems from an increase in water vapor pressure at saturation due to air warming and has been recently shown to drive decreases in plant productivity worldwide (see Chapter 1, Yuan et al., 2019; Lopez et al., 2021).

For soybean, increases in VPD, particularly between 60 and 90 days after sowing have been shown to be the most important drivers of yield variation in a yield trial dataset that spanned 27 U.S. states from 2007 to 2016, and this effect was detected even in the Upper Midwest, including Minnesota (Mourtzinis et al., 2019). While the effects of VPD on plant physiology are complex and still poorly understood (Grossiord et al., 2020; Lopez et al., 2021), it is widely accepted that negative VPD effects on soybean yields are at least partly driven by increases in crop water needs due to transpiration rate (TR) increase (Fletcher et al., 2007; Sadok and Sinclair, 2009a.b, Sinclair et al., 2010). Because crop productivity is constrained by water availability, increases in TR that are not matched by adequate supply through precipitation or irrigation often result in yield penalties, even in environments that are

considered well-watered, due to the extreme sensitivity of seed fill even to transient water deficit events (Sinclair et al., 2010).

In Minnesota, the simulation analysis of Sinclair et al. (2010) indicated that introducing soybean genotypes equipped with a limited transpiration rate trait would increase yields by up to 150 g m^{-2} with high probability (>0.95%), which indicates that yields are generally water-limited across most production systems in the state. In this systems analysis, the restriction of TR above a VPD threshold of 2 kPa to a constant rate resulted in yield increase by enabling a 'water conservation' behavior that resulted in an increase in stored soil moisture available during seed fill, thereby increasing yields. This behavior was first reported in a slow-wilting soybean line PI 146937, which has been used a donor line to various breeding programs across the U.S. (Carter et al., 2016; Ye et al., 2020). Alternatively, genotypes exhibiting an increase in TR under high VPD would be beneficial in environments or years where precipitation and soil moisture capacity are not limiting (Tamang et al., 2019; Sadok et al., 2019).

The physiological basis of this water-saving behavior in soybean has been shown to be driven by a hydraulic limitation of water transport in the leaves of soybean between the xylem and the guard cells (Sinclair et al., 2008). This hydraulic restriction has subsequently been linked to a lack of silver-sensitive aquaporin population that mediates cell-to-cell water movement in the mesophyll of the leaves of the slow-wilting genotype PI 416937 (Sadok and Sinclair, 2010a). Using this information, efforts have been undertaken to screen mapping populations based on a pharmacological approach consisting of feeding silver-based aquaporin inhibitors to

de-rooted plants, as an indirect way to identify the genetic basis of the water-conservation trait (Abdel-Haleem et al., 2012; Carpentieri-Pipolo et al., 2012; Steketee et al., 2019). However, a major challenge remains that such phenotyping approaches are based on using toxic chemicals and de-rooted plants and as a result, can have a number of side effects that could generate irrelevant trait-marker associations.

Directly phenotyping mapping populations for their TR response to VPD is a notoriously challenging effort that has not been successfully conducted so far. Since 2007, the cumulative number of phenotyped soybean genotypes for their TR response to VPD is under 60 (Fletcher et al., 2007; Sinclair et al., 2008; Sadok and Sinclair, 2009a.b; Seversike et al., 2014; Devi et al., 2014). This is mainly due to the complex logistics of reliably tracking whole-plant TR using a large number of balances, imposing VPD changes consistently across experiments, minimizing interaction with other confounding environmental variables, and ensuring that watering regimes are highly consistent across genotypes of various water needs. To address this challenge, a gravimetric screening system was designed to phenotype high-resolution TR response curves to VPD for entire mapping population, which has been successfully tested on maize (Tamang and Sadok, 2018), wheat (Tamang et al., 2019), and barley (Sadok and Tamang, 2019).

The first objective of this research is therefore to characterize the extent of genotypic variability in TR response to VPD in a mapping population consisting of 140 recombinant inbred lines (RILs) grown under similar conditions. These lines are derived from a cross between a commercial line, IA3023, and LG94-1906, which were

identified based on a pilot experiment and were found to exhibit relatively contrasting TR response curves to VPD. The second objective was to conduct a genetic mapping approach to identify QTL controlling TR response to VPD in soybean for the first time. More specifically, the goal was to identify alleles that confer a water-saving response by restricting TR, as well as alleles that maximize TR under high VPD.

2. Materials and methods

2.1. Genetic material

The genetic material of this study consisted of 140 recombinant inbred lines (RILs) of soybean derived from a cross between parents IA3023 and LG03-3191, a line with diverse ancestry. This population, called NAM25, is part of the soybean nested association mapping panel (SoyNAM), which is composed of 40 important soybean varieties crossed to a common parent, IA3023, to develop 40 RIL populations (www.soybase.org/SoyNAM). The NAM25 population was selected based on a preliminary experiment where all 40 parents were screened for their TR response to VPD, where LG03-3191 exhibited a response that contrasted the most with that of the recurrent parent IA3023 (Tamang et al. Unpublished).

2.2. Experiments

2.2.1. Experimental design and growth conditions

The population of 140 RILs and their parents were phenotyped in two independent experiments conducted at St. Paul campus of the University of

Minnesota (44.9866° N, 93.1832° W) over 2 consecutive years (2018-2019), using a gravimetric phenotyping platform (GraPh system, Tamang and Sadok 2018). While the GraPh system is currently the highest throughput platform of its kind, it enables screening of no more than 54 plants simultaneously on a given day (18 genotypes replicated three times) under controlled environment conditions. Due to the logistics of the phenotyping (see below for details), this effort took place over 3 consecutive days in a given week, resulting in a throughput of 54 genotypes per week. Therefore, in order to phenotype a population of 140 RILs, three sequential plantings – one per week – were implemented in each experiment. Each group was composed of 45-50 lines and one of the two parents as checks. The experimental design was an augmented incomplete block design with planting date as block and one of the parental lines as check. In experiment Exp1 parent LG03-3191 was the check, while in experiment Exp2 parent IA3023 was the check.

Plants were grown for 28-44 days until they reached the V4 stage, in a glasshouse regulated for a minimal temperature of 18°C (Table 1), based on a protocol developed by Tamang et al. (2019). Briefly, seeds were planted at a depth of 2.5cm in 3.8-liter pots filled with a garden mix (35% organic compost, 25% course fibrous peat, 30% screened soil, and 10% course sand; Plaisted Companies Inc., Elkriver, MN, USA). Pot filling was achieved such that seeds were planted in pots filled with a uniform amount of soil. In each pot, three similarly sized and healthy seeds were placed into three equidistant holes in the center of the pot, and then covered with

powdered rhizobial inoculant of *Bradyrhizobium japonicum* (NDure, Cary, NC). All pots were then lightly watered and immediately covered with tarps to minimize water evaporation from the surface of the soil until seedlings emerged, on average 4 d after planting.

One week following planting, each pot was given an equal amount of a slow-release fertilizer (15-9-12 NPK, Osmocote Plus, Miracle-Gro, Marysville, OH) along with a granular systemic insecticide (Marathon, OHP Inc., Bluffton, SC) to minimize thrips damage. Ten days after planting, pots were thinned from three to two plants, and three days later they were all thinned to one plant. Plants were watered at least twice weekly depending on plant size and evaporative conditions. On average during the growth period, pots were given 300 ml per irrigation event.

During the growth period, temperature (T), relative humidity (RH) and vapor pressure deficit (VPD) conditions inside the glasshouse were recorded every 5 mins with three portable USB sensors (Model EL-USB-2-LCD, Lascar Electronics, Whiteparish, UK) which were placed at canopy height in three different locations across the glasshouse (Table 1). Similarly, photosynthetically active radiation (PAR) was measured at canopy height using a quantum sensor (model S-LIA-M003, Onset Computer Corporation, Bourne, MA) connected to a data logger (HOBO H21-USB micro station, Onset computer Corporation, Bourne, MA) every 5 minutes to capture greenhouse growth conditions (Table 1). Plants were randomized in the glasshouse and rotated twice per week to minimize long-term effects on growth arising from spatial heterogeneity in PAR, T and VPD gradients across the glasshouse.

Table 1. Growth conditions subjected to the 140 recombinant inbred lines (RILs) during experiments Exp1 and Exp2. Given the size of the population relative to the phenotyping throughput, the population was split into three groups of 45-50 lines each, which were grown for 28-44 days prior to phenotyping. Averaged (± standard errors) daytime and nighttime conditions are presented for each group of lines.

		Daytime				**Nighttime**		
Exp.	Group	T (C°) ± SE	RH (%) ± SE	VPD (kPa) ± SE	PAR (µmol m^{-2} s^{-1}) ± SE	T (C°) ± SE	RH (%) ± SE	VPD (kPa) ± SE
Exp1 (June 2018)	1	32.8 ± 0.9	39.3 ± 2.1	3.3 ± 0.3	425 ± 23	21.6 ± 0.4	66.0 ± 2.1	0.9 ± 0.1
	2	32.2 ± 0.9	44.3 ± 2.5	3.0 ± 0.3	394 ± 26	22.2 ± 0.3	65.9 ± 0.3	0.9 ± 0.1
	3	32.0 ± 0.9	48.6 ± 2.9	2.8 ± 0.3	385 ± 31	22.8 ± 0.4	67.6 ± 0.4	0.9 ± 0.1
Exp2 (Nov 2019)	1	23.7 ± 0.3	45.7 ± 1.8	1.7 ± 0.1	238 ± 15	18.0 ± 0.2	57.0 ± 0.2	0.9 ± 0.0
	2	24.0 ± 0.2	48.3 ± 1.6	1.6 ± 0.1	204 ± 10	18.9 ± 0.2	56.9 ± 0.2	1.0 ± 0.0
	3	24.1 ± 0.3	43.4 ± 1.7	1.8 ± 0.1	210 ± 11	19.6 ± 0.0	49.4 ± 0.0	1.2 ± 0.0

2.2.2. Phenotyping transpiration rate response curves to increasing vapor pressure deficit

After growing in the glasshouse, plants were moved inside the GraPh platform following the procedure outlined in detail in Tamang et al. (2019). The platform consists of 54 high resolution balances (Model Fx-3000i, A & D Co. Ltd, Tokyo, Japan) protected from dust, moisture, vibration, and static electricity and connected to dataloggers which record changes in pot mass every minute at a resolution of a 0.01 g. These balances were placed inside 3 adjacent, identical, walk-in programmable growth chambers (Model PGV36, Conviron, Controlled Environments Ltd., Winnipeg, Manitoba, Canada), where target environmental conditions were imposed (Table 2). In these experiments, VPD changes were imposed over 7 consecutive steps where VPD was increased from 1.5 kPa to 3

kPa while temperature and PAR were kept constant at 30°C and approx. 500 μmol m^{-2} s^{-1}, respectively (Table 2). In each chamber, environmental conditions (T, RH, VPD, and PAR) at canopy level were continuously recorded every 5 min in 3 locations by the same sensors as described earlier.

Table 2. Temperature (T) and vapor pressure deficit (VPD) conditions imposed inside the GraPh platform during the phenotyping of transpiration rate (TR) response curves to increasing VPD of the 140 recombinant inbred lines (RILs) and their parents. For a given day, conditions are averaged across three growth chambers (3 sensors per chamber). Each VPD level is indicated with a number (1: lowest VPD; 7: highest VPD).

Exp.	Week	Day	T (°C) ± SE	VPD1 (kPa) ± SE	VPD2 (kPa) ± SE	VPD3 (kPa) ± SE	VPD4 (kPa) ± SE	VPD5 (kPa) ± SE	VPD6 (kPa) ± SE	VPD7 (kPa) ± SE
1	1	1	30.3 ± 0.02	1.5 ± 0.0	1.9 ± 0.0	2.3 ± 0.0	2.4 ± 0.0	2.6 ± 0.0	2.8 ± 0.0	2.9 ± 0.0
		2	30.3 ± 0.02	1.5 ± 0.0	1.7 ± 0.0	2.3 ± 0.0	2.5 ± 0.0	2.7 ± 0.0	2.9 ± 0.0	3.0 ± 0.0
		3	30.2 ± 0.03	1.4 ± 0.0	1.7 ± 0.0	2.2 ± 0.0	2.4 ± 0.0	2.6 ± 0.0	2.8 ± 0.0	2.9 ± 0.0
	2	1	30.4 ± 0.02	1.5 ± 0.0	1.8 ± 0.0	2.2 ± 0.0	2.4 ± 0.0	2.7 ± 0.0	2.9 ± 0.0	3.0 ± 0.0
		2	30.1 ± 0.02	1.5 ± 0.0	1.8 ± 0.0	2.2 ± 0.0	2.4 ± 0.0	2.6 ± 0.0	2.8 ± 0.0	3.0 ± 0.0
		3	30.3 ± 0.02	1.5 ± 0.0	1.9 ± 0.0	2.2 ± 0.0	2.5 ± 0.0	2.7 ± 0.0	3.0 ± 0.0	3.0 ± 0.0
	3	1	30.6 ± 0.02	1.5 ± 0.0	1.9 ± 0.0	2.3 ± 0.0	2.6 ± 0.0	2.7 ± 0.0	2.9 ± 0.0	3.0 ± 0.0
		2	30.3 ± 0.02	1.5 ± 0.0	1.9 ± 0.0	2.3 ± 0.0	2.5 ± 0.0	2.7 ± 0.0	2.9 ± 0.0	3.0 ± 0.0
		3	30.4 ± 0.01	1.5 ± 0.0	1.9 ± 0.0	2.2 ± 0.0	2.4 ± 0.0	2.6 ± 0.0	2.9 ± 0.0	3.1 ± 0.0
2	1	1	29.8 ± 0.01	1.4 ± 0.0	1.8 ± 0.0	2.0 ± 0.0	2.3 ± 0.0	2.5 ± 0.0	2.8 ± 0.0	3.0 ± 0.0
		2	29.9 ± 0.02	1.4 ± 0.0	1.8 ± 0.0	2.2 ± 0.0	2.4 ± 0.0	2.6 ± 0.0	2.9 ± 0.0	3.0 ± 0.0
		3	30.1 ± 0.03	1.5 ± 0.0	1.8 ± 0.0	2.3 ± 0.0	2.4 ± 0.0	2.6 ± 0.0	2.9 ± 0.0	3.1 ± 0.0
	2	1	29.9 ± 0.01	1.5 ± 0.0	1.9 ± 0.0	2.1 ± 0.0	2.4 ± 0.0	2.7 ± 0.0	2.9 ± 0.0	3.0 ± 0.0
		2	30.0 ± 0.02	1.5 ± 0.0	1.9 ± 0.0	2.1 ± 0.0	2.4 ± 0.0	2.7 ± 0.0	3.0 ± 0.0	3.1 ± 0.0
		3	29.8 ± 0.01	1.5 ± 0.0	1.8 ± 0.0	2.1 ± 0.0	2.3 ± 0.0	2.6 ± 0.0	2.9 ± 0.0	3.1 ± 0.0
	3	1	30.0 ± 0.01	1.5 ± 0.0	1.9 ± 0.0	2.1 ± 0.0	2.4 ± 0.0	2.7 ± 0.0	3.0 ± 0.0	3.1 ± 0.0
		2	29.8 ± 0.01	1.5 ± 0.0	1.9 ± 0.0	2.1 ± 0.0	2.4 ± 0.0	2.6 ± 0.0	2.9 ± 0.0	3.0 ± 0.0
		3	29.8 ± 0.01	1.4 ± 0.0	1.8 ± 0.0	2.1 ± 0.0	2.3 ± 0.0	2.6 ± 0.0	2.9 ± 0.0	3.1 ± 0.0

On the day preceding the phenotyping, plants were progressively watered until dripping and left to drain for approximately 6 hours, a period during which

pots were covered with aluminum foil, to nullify soil water evaporation. Thereafter, three replicates of each genotype were randomly placed on three balances across three growth chambers during the afternoon. During that time, plants were exposed to environmental conditions that are similar to the last day for a few hours, before exposing plants to uniform nighttime conditions (PAR = 0, T = 20°C and VPD = 1.0 kPa, dark period: 20:00h -06:00). The phenotyping started at 06:00 the next morning following the procedure fully detailed in Tamang et al. (2019). In summary, the seven target VPD settings were imposed for 60 min each, sequentially from the lowest to the highest, combining the use of industrial foggers and programmable de-humidifiers. At the end of the sequence, plants were removed from the platform and transferred to the lab where leaf areas were measured destructively using a leaf area meter (model LI3100-C, LiCOR, Lincoln, NE) so that transpiration rates account for differences in canopy size across genotypes. In total, approximately 450 plants per experiment were phenotyped using this system (i.e., a total of 900 plants).

2.3. Data analysis

2.3.1. Fitting transpiration rate response curves to increasing vapor pressure deficit

For each individual plant, values for TR were computed for each VPD step following Tamang and Sadok (2018). Three average TR and VPD values were calculated over a period of 45 mins (15 minutes each) for each 60 min step, as plants are likely to be acclimating to the new VPD regime during the first 15 min (Fletcher et

al. 2007; Schoppach and Sadok 2012). In total, the response curves of each genotype were fitted based on 63 data points (3 averages x 7 VPD steps × 3 replicate plants) in the 1.5–3 kPa VPD range, in each experiment.

In a first step, TR vs VPD regressions were first subjected to two fits: one linear and one segmented following Schoppach et al. (2016). When combining data from both experiments, this analysis revealed that a large group of genotypes (75%) were better described by a linear formalism while a segmented one applied best to the rest (25%). This made it unsuitable to use this fitting approach for phenotyping purposes due to the need for extracting the same phenotypic data from all genotypes to conduct the genetic mapping. Therefore, fitting TR vs VPD response curves was carried out using a quadratic model for all genotypes, as follows:

$$\mathrm{TR(VPD)} = \mathrm{aVPD}^2 + \mathrm{bVPD} + \mathrm{c}$$

Where the parameters a and b are the quadratic and linear terms of the model, respectively, and c is the y intercept. These fits were conducted using R scripts (R Core Team, 2021) using the nls function and the port algorithm (Bates and Watts, 1988). Using this equation, TR values at 1.5 and 3.0 kPa were approximated for each pot, i.e. TR(1.5) and TR(3). These values were used as phenotypic traits for genetic mapping. This quadratic approach is considered to be more biologically correct, reflecting both empirical and theoretical observations (Monteith, 1995; Eamus et al., 2008).

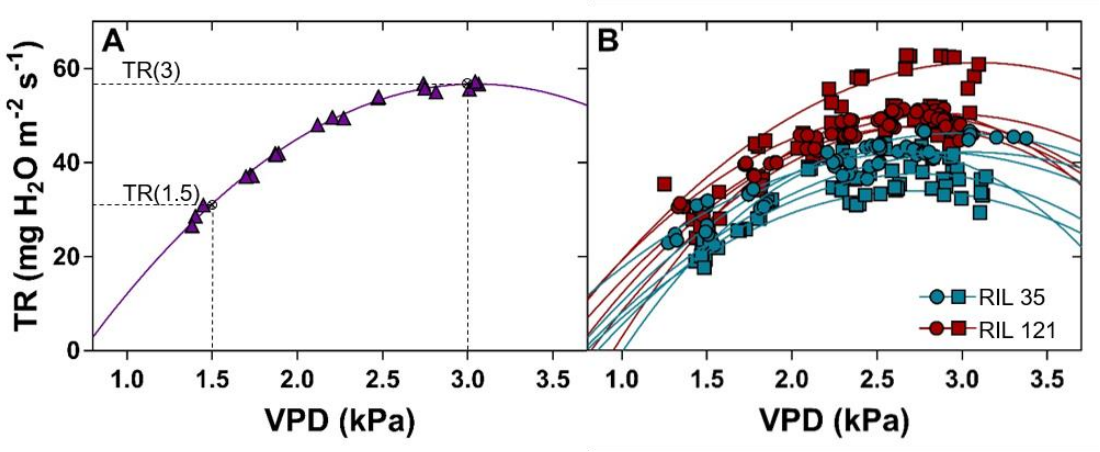

Figure 1. Example of quadratic fitting of TR response curves to increasing VPD for one replicate plant of a RIL (panel A) and for all replicates of 2 RILs (panel B). In panel A, dotted lines outline TR values estimated by the fitted model for VPD values of 1.5 (TR(1.5)) and 3.0 kPa (TR(3.0), see Materials and Methods for details). In panel B, the two RILs are distinguished by color, and experiment is distinguished by shape, with Exp1 and Exp2 shown as circles and squares, respectively.

2.3.2. QTL mapping

The Soy NAM population was genotyped and mapped using the SoyNAM6K Bead Chip developed for this population using the Illumina Infinium HD Assay platform (Illumina, Inc.) and made publicly available in the SoyBase data base (Grant et al., 2010; Song et al., 2017). Out of the 4312 single nucleotide polymorphism (SNP) markers found to be polymorphic and informative for the whole population, only 1534 markers were found to be polymorphic and informative for this population. Monomorphic markers, as well as contiguous markers exhibiting no recombination were filtered with the aid of the library qtl in R (Broman et al., 2003).

Quantitative trait loci (QTLs) were identified using the library qtl2 in R (Broman et al., 2019). The additive model was used to estimate marker probability and the leave one chromosome out (LOCO) method was used for the QTL analysis (Cobo et al., 2018). The population was simulated as an F5 advanced intercross. The logarithm of the odds (LOD) detection threshold was approximated through a permutation test with 1000 permutations. Confidence intervals for the QTLs were approximated using the 1.5 LOD approach. The coefficient of determination (R^2) and the additive effect of the QTLs were estimated through a linear least-squares regression of the phenotypic value on the QTL gene content (Lynch and Walsh, 1998).

3. Results

There was a substantial genetic variability in TR response curves to VPD in each experiment (Figure 2). The frequency distributions of parameter TR(1.5) and TR(3.0) were normal and relatively consistent across experiments, revealing similar ranges. Combining both experiments, TR(1.5) varied two-fold between genotypes, ranging from 19 to 38 mg H_2O m^{-2} s^{-1}, while parameter TR(3.0) exhibited a similar variation, although at a higher range (33 to 64 mg H_2O m^{-2} s^{-1}).

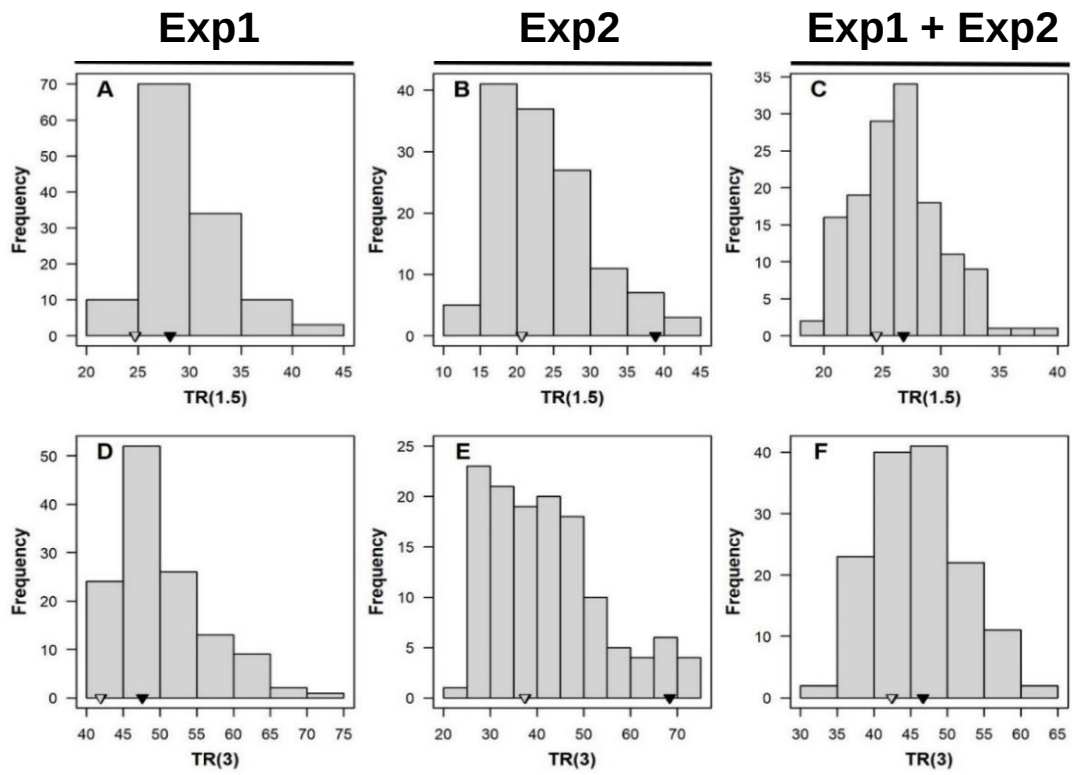

Figure 2. Frequency distributions for traits TR(1.5) and TR(3) in the RIL population. The experiments represented by each group of panels are reported above the panels. Values for the Hub parent, IA3023, are indicated with an open triangle and the values for the other parent, LG03-3191, are shown with a solid black triangle.

As illustrated in Figure 3, when combining both experiments, this variation translated into significant QTL for these traits. More specifically, two identical QTL were detected for TR(1.5) and TR(3.0), which are described in Table 3. For both parameters, the QTL detected are located in chromosomes 4 and 6, with a similar explained phenotypic variation (R^2) which ranged from 0.11 to 0.13. Irrespective of the trait, the QTL on chromosome 6 spanned a much smaller genetic distance (0.85 cM) compared to the one on chromosome 4 (52.3 cM). The chromosome 6 QTL also

exhibited the higher LOD score (5.02-5.33 vs 3.22-3.40) and a slightly lower additive effect compared to the one on chromosome 4 (Table 3). Independent from the chromosome, the additive effect of the QTL detected for TR(3.0) was higher (68% on average) relative to TR(1.5) (Table 3).

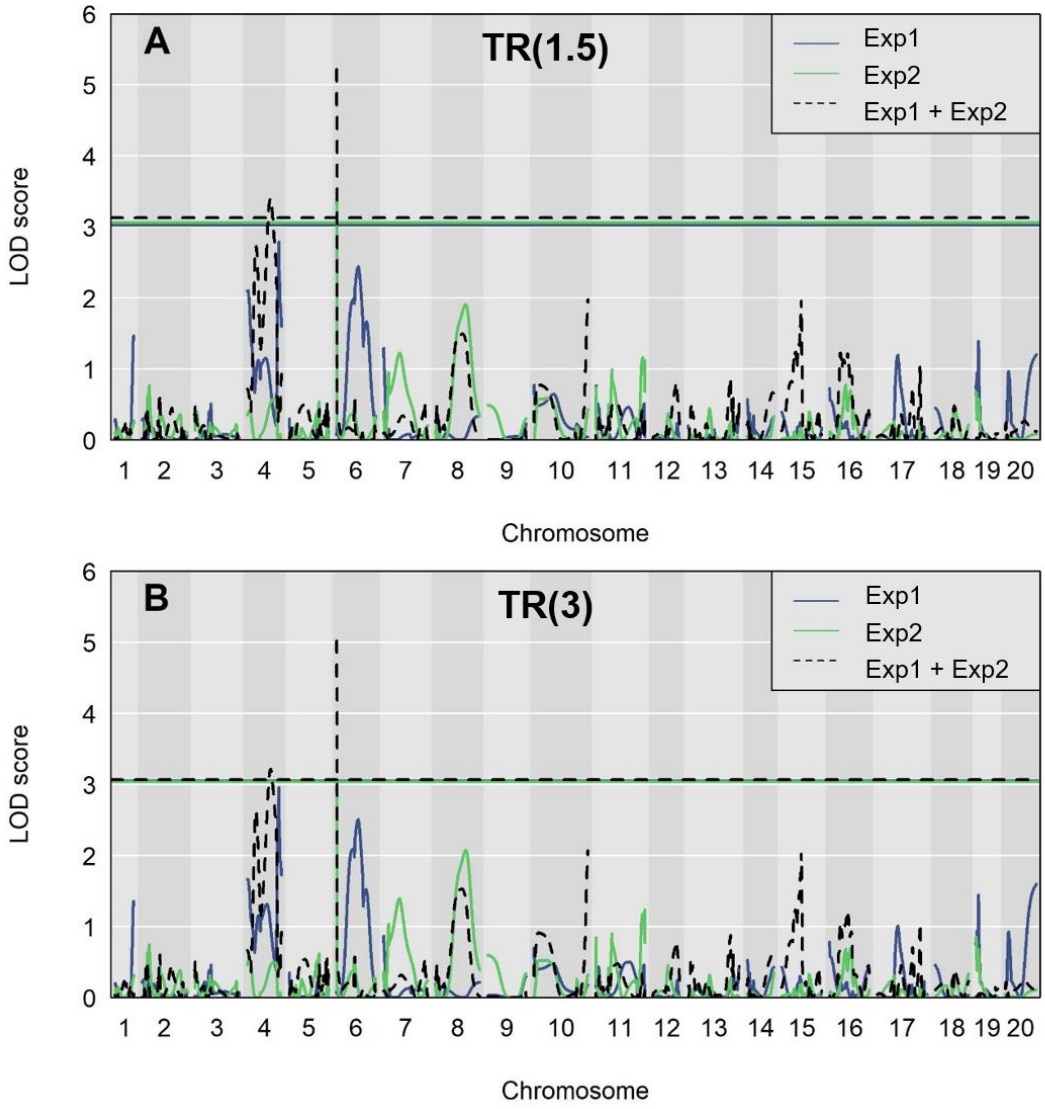

Figure 3. LOD score curves for QTL underlying traits TR(1.5, panel A) and TR(3, panel B) as a function of the experiment. Chromosomal positions are displayed on the x-axis and horizontal lines illustrate significance thresholds (LOD = 3).

Table 3. QTL mapping results for the traits TR(1.5) and TR(3) in the RIL population of the study. In the table, columns Chr, Pos and LOD respectively indicate the chromosome number, the position of the QTL on that chromosome in centiMorgans (cM), and the logarithm of the odds at the QTL location. Columns LL and UL represent the lower and upper confidence limit of 1.5 LOD interval, respectively. Effect indicates the additive effect (effect of one allele of the LG03-3191 parent), and R^2 indicates the coefficient of determination – the proportion of the phenotypic variation explained by the molecular markers.

Trait	**Chr**	**Pos**	**LL**	**UL**	**LOD**	**R^2**	**Effect**
TR(1.5)	4	66.51	28.99	81.25	3.40	0.13	-6.92E-05
	6	0	0	0.85	5.22	0.11	-6.28E-05
TR(3)	4	67.31	28.99	81.25	3.22	0.12	-1.15E-04
	6	0	0	0.85	5.02	0.11	-1.07E-04

4. Discussion

Plant water use is largely driven by evaporative demand. As vapor pressure deficit increases over the course of the day (typically 4 to 6-fold on a sunny day), it drives a substantial increase in TR (Dai et al. 1992; Monteith 1995; Franks et al., 1997; Grossiord et al., 2020). This increase in TR drives nutrient uptake and canopy temperature homeostasis, which are favorable for carbon fixation (Nobel, 1999; Novák and Vidovič, 2003; Lin et al., 2017). Therefore, in an environment where available water is not limiting, such behavior should lead to higher yield or at least be neutral (Sinclair et al., 2017; Sadok et al., 2019). However, in a water-deficit prone environment, soybean genotypes exhibiting lower TR at high VPD will outperform those exhibiting a 'profligate' TR, by reducing the amount of water lost during the time of day when evaporative demand is the highest without completely closing stomata, so that photosynthesis can still proceed. This type of trait is incorporated in

this study as TR(3). Therefore, a soybean genotype equipped with alleles favoring a high TR(3) in water-limited environments would lead to yield penalties, while it would increase yields in environments where seed fill is unlikely to be exposed to soil moisture deficits. The QTL identified in this study, if confirmed, could be leveraged to design soybean varieties that are optimized for specific water availability regimes in order to maximize productivity (Sinclair et al. 2010; Ye et al. 2020).

Despite progress in phenotyping soybean TR responses to increasing VPD, so far no QTL have been detected for traits directly reflecting such response curves, due to various methodological and logistical challenges. The QTL mapping performed here on the SoyNAM population NAM25 resulted in the detection, for the first time, of two QTL for the response of TR to both low and high VPD, TR(1.5) and TR(3) respectively (Figure 3, Table 3). The QTL identified are not yet confirmed, but serve as a basis for developing genetic knowledge about soybean control of transpiration in response to increasing VPD. In this regard, it is noteworthy that a recent QTL mapping effort in soybean identified slow-wilting (SW) QTL on the same chromosomes identified in our study, based on 2 mapping populations each having a donor parent exhibiting SW in the field (Ye et al. 2020). Critically, these two parents also exhibited a limited TR under high VPD, in alignment with our study (Ye et al. 2020).

The relatively limited number of QTL detected in this study could be explained by several factors. One would be the logistical constraints associated with the phenotyping effort, which translated in a sequential screening approach.

Concomitantly phenotyping the entire mapping population implies tracking whole-plant water use on more than 450 plants by simultaneously using balances, an approach that is currently cost-prohibitive (Tamang and Sadok 2018). As a result, our experiment necessitated three weekly sequential plantings as outlined in the materials and methods, which introduces the potential for developmental differences between the three planting groups as greenhouse conditions will not be exactly uniform across groups. Additionally, undesired plant husbandry factors likely played a role. For instance, significant germination issues exhibited by certain genotypes and thrips infestations that more severely affected certain plants than others may have generated additional variability that limited the range of detectable QTL.

Another key factor consists of the genetic structure of the mapping population. This population was not selected specifically because of highly contrasting parental phenotypes. It was chosen from a pool of available NAM populations for which genomic data was available, although within the SoyNAM panel the parents relatively contrasted in their TR response to VPD during a pilot experiment, as mentioned in the methods. Perhaps QTL could be found in greater resolution or quantity if a population was constructed from two highly contrasting parental varieties which could create more diverse progeny for QTL mapping, although that requires a much greater effort including breeding, genotyping, and linkage map construction.

Finally, our phenotyping approach focused solely on VPD as the key environmental variable, in order to reduce interactions with undesired sources of environmental variation such as light, temperature, and wind, which non-linearly

impact TR. This purposeful strategy might have contributed to reducing the number of QTL found.

A follow-up step in the investigation of the genetic basis of soybean TR response to VPD would be to confirm presence of the identified QTL in a different genetic background that maximizes potential allelic diversity for this trait, and to continue improving the phenotyping approach to resolve some limitations highlighted above. Alternatively, a validation step would be to screen heterogenous inbred families (HIFs) that segregate for the region of interest (Tuinstra et al. 1997) and see if they display differential TR response curves to VPD as predicted by their alleles, or even conduct yield trials under both limited and non-limited water availability.

Overall, and despite these limitations, this study is the first in any species where QTL mapping was conducted on TR response curves to VPD independent from other confounding environmental variables, and opens the way for identifying alleles maximizing soybean yield under increasing evaporative demand. The results of this research propose a possible genetic basis of transpiration rate response to increasing VPD, and despite the unconfirmed nature of the QTL, it invites future studies to for validation or to identify other, new QTL.

BIBLIOGRAPHY

Abdel-Haleem H, Carter TE, Purcell LC *et al.* 2012. Mapping of quantitative trait loci for canopy-wilting trait in soybean (*Glycine max* L. Merr). *Theoretical and Applied Genettics* **125**, 837–846. https://doi.org/10.1007/s00122-012-1876-9

Annan H, Golding A-L, Zhao Y, Dong Z. 2012. Choice of hydrogen uptake (Hup) status in legume-rhizobia symbioses. *Ecology and Evolution* **2** (9): 2285–2290. https://doi.org/10.1002/ece3.325

Bacanamwo M, Harper JE. 1997. The feedback mechanism of nitrate inhibition of nitrogenase activity in soybean may involve asparagine and/or products of its metabolism. *Physiologia Plantarum* **100**, 371-377. https://doi.org/10.1111/j.1399-3054.1997.tb04795.x

Bates DM, Watts DG. 1988. Nonlinear regression analysis and its applications. Hoboken, NJ, USA. John Wiley & Sons.

Boyer JS. 1982. Plant Productivity and Environment. *Science* **218**, 443-448. http://dx.doi.org/10.1126/science.218.4571.443

Broman KW, Gatti DM, Simecek P, Furlotte NA, Prins P, Sen Ś, Yandell YS, Churchill GA. 2019. R/qtl2: Software for Mapping Quantitative Trait Loci with High-Dimensional Data and Multiparent Populations. *Genetics* **211** (2, 1): 495–502. https://doi.org/10.1534/genetics.118.301595

Broman KW, Wu H, Sen Ś, Churchill GA. 2003. R/qtl: QTL mapping in experimental crosses. *Bioinformatics* **19** (7), 889–890. https://doi.org/10.1093/bioinformatics/btg112

Carpentieri-Pipolo V, Pipolo AE, Abdel-Haleem H, Boerma HR, Sinclair TR. 2012. Identification of QTLs associated with limited leaf hydraulic conductance in soybean. *Euphytica* **186**, 679–686. https://doi.org/10.1007/s10681-011-0535-6

Carson P. 2002. Hazardous Chemicals Handbook. 2nd edition. Butterworth-Heinemann.

Carter TE, Todd SM, Gillen AM. 2016. Registration of 'USDA-N8002' Soybean Cultivar with High Yield and Abiotic Stress Resistance Traits. *Journal of Plant Registrations* **10**, 238-245. https://doi.org/10.3198/jpr2015.09.0057crc

Chenu K, Deihimfard R, Chapman SC. 2013. Large-scale characterization of drought pattern: a continent-wide modelling approach applied to the Australian wheatbelt – spatial and temporal trends. *New Phytology* **198**, 801-820. https://doi.org/10.1111/nph.12192

Cobo N, Pflüger L, Chen X, Dubcovsky J. 2018. Mapping QTL for Resistance to New Virulent Races of Wheat Stripe Rust from Two Argentinean Wheat Cultivars. *Crop Science* **58**, 2470-2483**.** https://doi.org/10.2135/cropsci2018.04.0286

Da Silva MC, Shelp BJ. 1990. Xylem-to-Phloem Transfer of Organic Nitrogen in Young Soybean Plants. *Plant Physiology* **92** (3), 797–801. https://doi.org/10.1104/pp.92.3.797

Dai A, Zhao T, Chen J. 2018. Climate change and drought: a precipitation and evaporation perspective. *Current Climate Change Reports* **4** (3), 301–312. https://doi.org/10.1007/s40641-018-0101-6

Dai A. 2013. Increasing drought under global warming in observations and models. *Nature Climate Change* **3**, 52–58. https://doi.org/10.1038/nclimate1633

Dai Z, Edwards GE, Ku MSB. 1992. Control of Photosynthesis and Stomatal Conductance in *Ricinus communis* L. (Castor Bean) by Leaf to Air Vapor Pressure Deficit. *Plant Physiology* **99** (4), 1426-1434. https://doi.org/10.1104/pp.99.4.1426

de Silva M, Purcell LC, King CA. 1996. Soybean Petiole Ureide Response to Water Deficits and Decreased Transpiration. *Crop Science* **36**, 611-616. https://doi.org/10.2135/cropsci1996.0011183X003600030015x

Denison RF, Sinclair TR, Zobel RW *et al.* 1983. A non-destructive field assay for soybean nitrogen fixation by acetylene reduction. *Plant and Soil* **70**, 173–182. https://doi.org/10.1007/BF02374778

Denison RF, Sinclair TR. 1985. Diurnal and Seasonal Variation in Dinitrogen Fixation (Acetylene Reduction) Rates by Field–Grown Soybeans. *Agronomy Journal* **77**, 679-684. https://doi.org/10.2134/agronj1985.00021962007700050005x

Denison RF, Weisz PR, Sinclair TR. 1988. Oxygen supply to nodules as a limiting factor in symbiotic nitrogen fixation. In: Summerfield R.J. (eds) World crops: Cool season food legumes. *Current Plant Science and Biotechnology in Agriculture* **5**. Springer, Dordrecht. https://doi.org/10.1007/978-94-009-2764-3_61

Devi JM, Sinclair TR, Chen P, Carter TE. 2014. Evaluation of Elite Southern Maturity Soybean Breeding Lines for Drought-Tolerant Traits. *Agronomy Journal* **106**, 1947-1954. https://doi.org/10.2134/agronj14.0242

Durand JL, Sheehy JE, Minchin FR. 1987. Nitrogenase Activity, Photosynthesis and Nodule Water Potential in Soyabean Plants Experiencing Water Deprivation. *Journal of Experimental Botany* **38** (2), 311–321. https://doi.org/10.1093/jxb/38.2.311

Eamus D, Taylor DT, Macinnis-Ng CMO, Shanahan S, de Silva L. 2008. Comparing model predictions and experimental data for the response of stomatal conductance and guard cell turgor to manipulations of cuticular conductance, leaf-to-air vapour pressure difference and temperature: feedback mechanisms are able to account for all observations. *Plant, Cell and Environment* **31**, 269–277. https://doi.org/10.1111/j.1365-3040.2007.01771.x

Evans HJ, Harker AR, Papen H, Russell SA, Hanus FJ, Zuber M. 1987. Physiology, biochemistry, and genetics of the uptake hydrogenase in rhizobia. *Annual Review of Microbiology* **41**, 335-361. https://doi.org/10.1128/JB.183.8.2595-2604.2001

Ficklin DL, Novick KA. 2017. Historic and projected changes in vapor pressure deficit suggest a continental-scale drying of the United States atmosphere. *Journal of Geophysical Research: Atmospheres* **122**, 2061– 2079. https://doi.org/10.1002/2016JD025855

Fletcher AL, Sinclair TR, Allen LH. 2007. Transpiration responses to vapor pressure deficit in well watered 'slow-wilting' and commercial soybean. *Environmental and Experimental Botany* **61** (2), 145-151. https://doi.org/10.1016/j.envexpbot.2007.05.004.

Franks PJ, Cowan IR, Farquhar GD. 1997. The apparent feedforward response of stomata to air vapour pressure deficit: information revealed by different experimental procedures with two rainforest trees. *Plant, Cell & Environmen*t **20**, 142–145. https://doi.org/10.1046/j.1365-3040.1997.d01-14.x

Fujikake H, Yashima H, Sato T, Ohtake N, Sueyoshi K, Ohyama T. 2002. Rapid and reversible nitrate inhibition of nodule growth and N2 fixation activity in soybean (*Glycine max (L.) Merr*.). *Soil Science and Plant Nutrition* **48**, 211–217. https://doi.org/10.1080/00380768.2002.10409193

Grant D, Nelson RT, Cannon SB, Shoemaker RC. 2010. SoyBase, the USDA-ARS soybean genetics and genomics database. *Nucleic Acids Research* 38, 843–846. https://doi.org/10.1093/nar/gkp798

Grossiord C, Buckley TN, Cernusak LA, Novick KA, Poulter B, Siegwolf RTW, Sperry JS, McDowell NG. 2020. Plant responses to rising vapor pressure deficit. *New Phytology* **226**, 1550-1566. https://doi.org/10.1111/nph.16485

Hardy RWF, Holsten RD, Jackson EK, Burns RC. 1968. The Acetylene-Ethylene Assay for N2 fixation: laboratory and field evaluation. *Plant Physiology* **43**, 1185–1207. https://doi.org/10.1104/pp.43.8.1185

Henchion M, Hayes M, Mullen AM, Fenelon M, Tiwari B. 2017. Future Protein Supply and Demand: Strategies and Factors Influencing a Sustainable Equilibrium. *Foods* **6** (7), 53. https://doi.org/10.3390/foods6070053

Hunt S, Layzell DB. 1993. Gas Exchange of Legume Nodules and the Regulation of Nitrogenase Activity. *Annual Review of Plant Physiology and Plant Molecular Biology* **44**(1), 483-511. https://doi.org/10.1146/annurev.pp.44.060193.002411

Johnson HS, Hume DJ. 1972. Effects of nitrogen sources and organic matter on nitrogen fixation and yield of soybeans. *Canadian Journal of Plant Science* **52** (6), 991-996. https://doi.org/10.4141/cjps72-170

Jung M, Reichstein M, Ciais P. *et al.* 2010. Recent decline in the global land evapo-transpiration trend due to limited moisture supply. *Nature* **467**, 951–954. https://doi.org/10.1038/nature09396

King CA, Purcell LC. 2005. Inhibition of N2 Fixation in Soybean Is Associated with Elevated Ureides and Amino Acids. *Plant Physiology* **137** (4), 1389-1396. https://doi.org/10.1104/pp.104.056317

Kuzma MM, Layzell DB. 1994. Acclimation of Soybean Nodules to Changes in Temperature. *Plant Physiology* **106** (1), 263-270. https://doi.org/10.1104/pp.106.1.263

La Favre JS, Focht DD. 1983. Conservation in soil of H_2 liberated from N_2 fixation by Hup^- nodules. *Applied and Environmental Microbiology* **46** (2), 304–311. https://doi.org/10.1128/aem.46.2.304-311.1983

Lin H, Chen Y, Zhang H, Fu P, Fan Z. 2017. Stronger cooling effects of transpiration and leaf physical traits of plants from a hot dry habitat than from a hot wet habitat. *Functional Ecology* **31**, 2202– 2211. https://doi.org/10.1111/1365-2435.12923

Liu W, Sun F. 2017. Projecting and attributing future changes of evaporative demand over China in CMIP5 climate models. *Journal of Hydrometeorology* **18** (4), 977–991. https://doi.org/10.1175/JHM-D-16-0204.1

Lobell DB, Schlenker W, Costa-Roberts J. 2011. Climate Trends and Global Crop Production Since 1980. *Science* **333** (6042), 616-620. https://doi.org/10.1126/science.1204531

Lopez J, Way DA, Sadok W. 2021. Systemic effects of rising atmospheric vapor pressure deficit on plant physiology and productivity. *Global Change Biology* **27**, 1704-1720. https://doi.org/10.1111/gcb.15548

Lynch M, Walsh B. (1998). Genetics and Analysis of Quantitative Traits. Sinauer Associates: Sunderland, MA. https://doi.org/10.1046/j.1439-0388.2002.00356.x

Maimaiti J, Zhang Y, Yang J, Cen Y-P, Layzell DB, Peoples M, Dong Z. 2007. Isolation and characterization of hydrogen-oxidizing bacteria induced following exposure of soil to hydrogen gas and their impact on plant growth. *Environmental Microbiology* **9**, 435-444. https://doi.org/10.1111/j.1462-2920.2006.01155.x

Matiu M, Ankerst DP, Menzel A. 2017. Interactions between temperature and drought in global and regional crop yield variability during 1961-2014. *PLOS ONE* **12** (5), e0178339. https://doi.org/10.1371/journal.pone.0178339

Minchin FR, Sheehy JE, Witty JF. 1986. Further Errors in the Acetylene Reduction Assay: Effects of Plant Disturbance. *Journal of Experimental Botany* 37 (10), 1581–1591. https://doi.org/10.1093/jxb/37.10.1581

Minchin FR, Witty JF, Sheehy JE, Müller M. 1983. A Major Error in the Acetylene Reduction Assay: Decreases in Nodular Nitrogenase Activity Under Assay Conditions. *Journal of Experimental Botany* **34** (142): 641-649. https://doi.org/10.1093/jxb/34.5.641

Minchin FR, Sheehy JE, Witty JF. 1985. Factors Limiting N2 Fixation by the Legume-Rhizobium Symbiosis. In: Evans HJ, Bottomley PJ, Newton WE. (eds) Nitrogen fixation research progress. *Current Plant Science and Biotechnology in Agriculture* **1**. Springer, Dordrecht. https://doi.org/10.1007/978-94-009-5175-4_40

Monteith JL. 1995. A reinterpretation of stomatal responses to humidity. *Plant, Cell & Environment* **18**, 357-364. https://doi.org/10.1111/j.1365-3040.1995.tb00371.x

Mourtzinis S, Specht JE, Conley SP. 2019. Defining Optimal Soybean Sowing Dates across the US. *Scientific Reports* **9**, 2800. https://doi.org/10.1038/s41598-019-38971-3

Mourtzinis S, Specht J, Lindsey L. *et al.* 2015. Climate-induced reduction in US-wide soybean yields underpinned by region- and in-season-specific responses. *Nature Plants* **1**, 14026. https://doi.org/10.1038/nplants.2014.26

Nobel PS. 1999. Physiochemical and Environmental Plant Physiology. Academic Press, London.

Noel KD, Carneol M, Brill WJ. 1982. Nodule Protein Synthesis and Nitrogenase Activity of Soybeans Exposed to Fixed Nitrogen. *Plant Physiology* **70** (5), 1236-1241. https://doi.org/10.1104/pp.70.5.1236

Novák V, Vidovič J. 2003. Transpiration and nutrient uptake dynamics in maize (Zea mays L.). *Ecological Modelling* **166** (1–2), 99-107 https://doi.org/10.1016/S0304-3800(03)00102-9

Oono R, Denison RF. 2010. Comparing symbiotic efficiency between swollen versus nonswollen rhizobial bacteroids. *Plant Physiology* **154** (3), 1541-1548. https://doi.org/10.1104/pp.110.163436

Oono R, Muller KE, Ho R, Salinas AJ, Denison RF. 2020. How do less-expensive nitrogen alternatives affect legume sanctions on rhizobia? *Ecology and Evolution* **10**, 10645-10656. https://doi.org/10.1002/ece3.6718

Parsons R, Ravens JA, Sprent JI. 1992. A Simple Open Flow System Used to Measure Acetylene Reduction Activity of Sesbania rostrata Stem and Root Nodules. *Journal of Experimental Botany* **43** (250), 595-604. https://doi.org/10.1093/jxb/43.5.595

Parsons R, Stanforth A, Raven JA, Sprent JI. 1993. Nodule growth and activity may be regulated by a feedback mechanism involving phloem nitrogen. *Plant, Cell & Environment* **16**, 125-136. https://doi.org/10.1111/j.1365-3040.1993.tb00854.x

Pratap A, Gupta SK, Kumar J, Solanki RK. 2012. Soybean. In: Gupta S. (eds) Technological Innovations in Major World Oil Crops **1**, Springer, New York, NY. https://doi.org/10.1007/978-1-4614-0356-2_12

R Core Team. 2021. R: A language and environment for statistical computing. *R Foundation for Statistical Computing.* http://www.r-project.org/

Ray DK, West PC, Clark M, Gerber JS, Prishchepov AV. *et al.* 2019. Climate change has likely already affected global food production. *PLOS ONE* **14** (5), e0217148. https://doi.org/10.1371/journal.pone.0217148

Riar M, Cerezini P, Manandhar A, Sinclair TR, Li Z, Carter T. 2018. Expression of Drought-Tolerant N Fixation in Heterogeneous Inbred Families derived from PI471938 and Hutcheson Soybean. *Crop Science* **58**, 364-369.

Sadok W, Schoppach R, Ghanem ME, Zucca C, Sinclair TR. 2019. Wheat drought-tolerance to enhance food security in Tunisia, birthplace of the Arab spring. *European Journal of Agronomy* **107**, 1–9. https://doi.org/10.1016/j.eja.2019.03.009

Sadok W, Sinclair TR. 2009a. Genetic Variability of Transpiration Response to Vapor Pressure Deficit among Soybean Cultivars. *Crop Science* **49**, 955-960. https://doi.org/10.2135/cropsci2008.09.0560

Sadok W, Sinclair TR. 2009b. Genetic variability of transpiration response to vapor pressure deficit among soybean (*Glycine max* [L.] Merr.) genotypes selected from a recombinant inbred line population. *Field Crops Research* **113** (2), 156-160. https://doi.org/10.1016/j.fcr.2009.05.002

Sadok W, Sinclair TR. 2010a. Transpiration response of 'slow-wilting' and commercial soybean (*Glycine max (L.) Merr.)* genotypes to three aquaporin inhibitors. *Journal of Experimental Botany* **61** (3), 821–829. https://doi.org/10.1093/jxb/erp350

Sadok W, Sinclair TR. 2010b. Genetic Variability of Transpiration Response of Soybean [*Glycine max* (L.) Merr.] Shoots to Leaf Hydraulic Conductance Inhibitor $AgNO_3$. *Crop Science* **50**, 1423-1430. https://doi.org/10.2135/cropsci2009.10.0575

Sadok W, Tamang BG. 2019. Diversity in daytime and night-time transpiration dynamics in barley indicates adaptation to drought regimes across the Middle-East. *Journal of Agronomy and Crop Science* **205**, 372– 384. https://doi.org/10.1111/jac.12331

Sall K, Sinclair TR. 1991. Soybean genotypic differences in sensitivity of symbiotic nitrogen fixation to soil dehydration. *Plant and Soil* **133**, 31–37. https://doi.org/10.1007/BF00011896

Schoppach R, Sadok W. 2012. Differential sensitivities of transpiration to evaporative demand and soil water deficit among wheat elite cultivars indicate different strategies for drought tolerance. *Environmental and Experimental Botany* **84**, 1-10. https://doi.org/10.1016/j.envexpbot.2012.04.016.

Schoppach R, Taylor JD, Majerus E, Claverie E, Baumann U, Suchecki R, Fleury D, Sadok W. 2016. High resolution mapping of traits related to whole-plant transpiration under increasing evaporative demand in wheat. *Journal of Experimental Botany* **67** (9), 2847–2860. https://doi.org/10.1093/jxb/erw125

Schuler S, Conrad R. 1991. Hydrogen oxidation in soil following rhizobial H2 production due to N2 fixation by a Vicia faba-Rhizobium leguminosarum symbiosis. *Biology and Fertility of Soils* **11**, 190-195. https://doi.org/10.1007/BF00335766

Serraj R, Sinclair TR. 1996. Inhibition of nitrogenase activity and nodule oxygen permeability by water deficit. *Journal of Experimental Botany* **47** (8), 1067–1073. https://doi.org/10.1093/jxb/47.8.1067

Serraj R, Sinclair TR. 1997. Variation among Soybean Cultivars in Dinitrogen Fixation Response to Drought. *Agronomy Journal* **89**, 963-969. https://doi.org/10.2134/agronj1997.00021962008900060019x

Serraj R, Vadez V, Denison RF, Sinclair TR. 1999. Involvement of ureides in nitrogen fixation inhibition in soybean. *Plant Physiology* **119**, 289–296. https://doi.org/10.1104/pp.119.1.289

Seversike TM, Sermons SM, Sinclair TR, *et al.* 2014. Physiological properties of a drought-resistant wild soybean genotype: Transpiration control with soil drying and expression of root morphology. *Plant and Soil* **374,** 359–370. https://doi.org/10.1007/s11104-013-1757-2

Silvester WB, Parsons R, Minchin FR, Witty JF. 1989. Simple Apparatus for Growth of Nodulated Plants and for Continuous Nitrogenase Assay Under Defined Gas Phase. In: Torrey J.G., Winship L.J. (eds) Applications of Continuous and Steady-State Methods to Root Biology. *Developments in Plant and Soil Sciences* **34**. Springer, Dordrecht. https://doi.org/10.1007/978-94-009-2237-2_3

Sinclair TR. 1986. Water and nitrogen limitations in soybean grain production I. Model development. *Field Crops Research* **15** (2), 125-141. https://doi.org/10.1016/0378-4290(86)90082-1

Sinclair TR. 2012. Is transpiration efficiency a viable plant trait in breeding for crop improvement? *Functional Plant Biology* **39** (5), 359-365 https://doi.org/10.1071/FP11198

Sinclair TR, Bennett JM. 1998. Water. In: Sinclair TR, Gardner FP. (Eds.), *Principles of Ecology in Plant Production*, 103–120.

Sinclair TR, Serraj R. 1995. Legume nitrogen fixation and drought. *Nature* **378**, 344 https://doi.org/10.1038/378344a0

Sinclair TR, Devi J, Shekoofa A *et al.* 2017. Limited-transpiration response to high vapor pressure deficit in crop species. *Plant Science* **260**, 109–118. https://doi.org/10.1016/j.plantsci.2017.04.007

Sinclair TR, Messina CD, Beatty A, Samples M. 2010. Assessment across the United States of the Benefits of Altered Soybean Drought Traits. *Agronomy Journal* **102**, 475-482. https://doi.org/10.2134/agronj2009.0195

Sinclair TR, Purcell LC, King CA, Sneller CH, Chen P, Vadez V. 2007. Drought tolerance and yield increase of soybean resulting from improved symbiotic N2 fixation. *Field Crops Research* **101** (1), 68-71. https://doi.org/10.1016/j.fcr.2006.09.010

Sinclair TR, Zwieniecki MA, Holbrook NM. 2008. Low leaf hydraulic conductance associated with drought tolerance in soybean. *Physiologia Plantarum*, **132** (4), 446-451. https://doi.org/10.1111/j.1399-3054.2007.01028.x

Smercina DN, Evans SE, Friesen ML, Tiemann LK. 2019. Optimization of the $^{15}N_2$ incorporation and acetylene reduction methods for free-living nitrogen fixation. *Plant and Soil* **445**, 595–611. https://doi.org/10.1007/s11104-019-04307-3

Smith AG, Han E, Petersen J, Faircloth AN, Giese C, Athmann M, Dresbøll DB, Thorup-Kristensen K. 2020. RootPainter: Deep Learning Segmentation of

Biological Images with Corrective Annotation. *bioRxiv*. https://doi.org/10.1101/2020.04.16.044461

Song Q, Yan L., Quigley C, Jordan BD, Fickus E, Schroeder S, Song BH, Charles An Y-Q, Hyten D, Nelson R, Rainey K, Beavis WD, Specht J, Diers B, Cregan P. 2017. Genetic Characterization of the Soybean Nested Association Mapping Population. *The Plant Genome* **10**, plantgenome2016.10.0109 https://doi.org/10.3835/plantgenome2016.10.0109

Steketee CJ, Sinclair TR, Riar MK *et al.* 2019. Unraveling the genetic architecture for carbon and nitrogen related traits and leaf hydraulic conductance in soybean using genome-wide association analyses. *BMC Genomics* **20**, 811. https://doi.org/10.1186/s12864-019-6170-7

Tamang BG, Sadok W. 2018. Nightly business: Links between daytime canopy conductance, nocturnal transpiration and its circadian control illuminate physiological trade-offs in maize. *Environmental and Experimental Botany*. **148**, 192-202, https://doi.org/10.1016/j.envexpbot.2017.11.016.

Tamang BG, Schoppach R, Monnens D, Steffenson BJ, Anderson JA, Sadok W. 2019. Variability in temperature-independent transpiration responses to evaporative demand correlate with nighttime water use and its circadian control across diverse wheat populations. *Planta* **250,** 115–127. https://doi.org/10.1007/s00425-019-03151-0

Tanner CB, Sinclair TR. 1983. Efficient Water Use in Crop Production: Research or Re-Search?. In Limitations to Efficient Water Use in Crop Production (editors: Taylor HM, Jordan WR, Sinclair TR). https://doi.org/10.2134/1983.limitationstoefficientwateruse.c1

Tardieu F, Simonneau T, Muller B. 2018. The physiological basis of drought tolerance in crop plants: a scenario-dependent probabilistic approach. *Annual Review of Plant Biology* **69**, 733–759. https://doi.org/10.1146/annurev-arplant-042817-040218

Teixeira EI, Fischer G, van Velthuizen H, Walter C, Ewert F. 2013. Global hot-spots of heat stress on agricultural crops due to climate change. *Agricultural and Forest Meteorology* **170,** 206-215. https://doi.org/10.1016/j.agrformet.2011.09.002.

Tonin P, Gosselet N, Halle E, Henrion M. 2018. Ideal oil and protein crops – what are users ideotypes, from the farmer to the consumer? *Oilseeds and fats, Crops and Lipids* **25** (6), D605. https://www.ocl-journal.org/articles/ocl/full_html/2018/06/ocl180060s/ocl180060s.html

Tuinstra M, Ejeta G, Goldsbrough P. 1997. Heterogeneous inbred family (HIF) analysis: a method for developing near-isogenic lines that differ at quantitative trait loci. *Theoretical and Applied Genetics* **95,** 1005–1011. https://doi.org/10.1007/s001220050654

United Nations. 2019. Revision of World Population Prospects, United Nations. Online:https://population.un.org/wpp/Publications/Files/WPP2019_10KeyFindings.pdf

USDA, FAS. 2021. Soybeans: World Supply and Distribution**.** [cited 15 April 2021]
USDA, FSA. 2020. 2020 acreage data as of December 10, 2020. [cited 15 April 2021]
Vadez V, Sinclair TR. 2001. Leaf ureide degradation and N_2 fixation tolerance to water deficit in soybean. *Journal of Experimental Botany* **52** (354), 153–159. https://doi.org/10.1093/jexbot/52.354.153

Vadez V, Sinclair TR, Serraj R. 2000. Asparagine and ureide accumulation in nodules and shoots as feedback inhibitors of N2 fixation in soybean. *Physiologia Plantarum* **110**, 215-223. https://doi.org/10.1034/j.1399-3054.2000.110211.x
Vessey J. 1994. Measurement of nitrogenase activity in legume root nodules: in defense of the acetylene reduction assay. *Plant and Soil* **158**, 151–162. https://doi.org/10.1007/BF00009490
Walch G, Opitz AK, Kogler S *et al*. 2014. Correlation between hydrogen production rate, current, and electrode overpotential in a solid oxide electrolysis cell with La0.6Sr0.4FeO3−δ thin-film cathode. *Monatsh Chem* **145**, 1055–1061. https://doi.org/10.1007/s00706-014-1220-y
Weisz PR, Sinclair TR. 1988. Soybean nodule gas permeability, nitrogen fixation and diurnal cycles in soil temperature. *Plant and Soil* **109**, 227–234. https://doi.org/10.1007/BF02202088
White PJ. 2012. Chapter 3 - Long-distance Transport in the Xylem and Phloem. Editor(s): Petra Marschner. Marschner's Mineral Nutrition of Higher Plants (Third Edition). *Academic Press*, 49-70. https://doi.org/10.1016/B978-0-12-384905-2.00003-0.
Wijewardana C, Reddy KR, Alsajri FA, *et al.* 2018. Quantifying soil moisture deficit effects on soybean yield and yield component distribution patterns. *Irrigation Science* **36**, 241–255. https://doi.org/10.1007/s00271-018-0580-1
Witty JF. 1991. Microelectrode Measurements of Hydrogen Concentrations and Gradients in Legume Nodules. *Journal of Experimental Botany* **42** (239), 765-77. https://doi.org/10.1093/jxb/42.6.765
Witty J, Minchin FR. 1998. Hydrogen measurements provide direct evidence for a variable physical barrier to gas diffusion in legume nodules. *Journal of Experimental Botany* **49** (323), 1015–1020. https://doi.org/10.1093/jexbot/49.323.1015
Ye H, Song L, Schapaugh WT, Ali ML, Sinclair TR, Riar MK, Mutava RN, Li Y, Vuong T, Valliyodan B, Neto AP, Klepadlo M, Song Q, Shannon JG, Chen P, Nguyen HT. 2020. The importance of slow canopy wilting in drought tolerance in soybean. *Journal of Experimental Botany* **71** (2), 642–652. https://doi.org/10.1093/jxb/erz150
Yuan W, Zheng Y, Piao S, Ciais P, Lombardozzi D, Wang Y, Ryu Y, Chen G, Dong W, Hu Z *et al*. 2019. Increased atmospheric vapor pressure deficit

reduces global vegetation growth. *Science Advances* **5**, eaax1396. https://doi.org/10.1126/sciadv.aax1396

Zampieri M, Ceglar A, Dentener F, Toreti A. 2017. Wheat yield loss attributable to heat waves, drought and water excess at the global, national and subnational scales. *Environmental Research Letters* **12** 064008. https://iopscience.iop.org/article/10.1088/1748-9326/aa723b

Zhang K, Kimball JS, Nemani RR, Running SW, Hong Y, Gourley JJ, Yu Z. 2015. Vegetation greening and climate change promote multidecadal rises of global land evapotranspiration. *Scientific Reports* **5**, 15956. https://doi.org/10.1038/srep15956

Zipper SC, Qiu J, Kucharik CJ. 2016. Drought effects on US maize and soybean production: Spatiotemporal patterns and historical changes. *Environmental Research Letters* **11**, 1–11. https://doi.org/10.1088/1748-9326/11/9/094021